Water Resources Research

RESEARCH ARTICLE
10.1029/2020WR027381

Utilization of Nonequilibrium Phase Change Approach to Analyze the Nonisothermal Multiphase Flow in Shallow Subsurface Soils

Mohammadreza Mir Tamizdoust[1] and **Omid Ghasemi-Fare**[1]

[1]Department of Civil and Environmental Engineering, University of Louisville, Louisville, KY, USA

Key Points:
- Nonequilibrium phase change is dominant for the very shallow subsurface soil with respect to dynamic variations of atmospheric demand
- Film flow and a general SWR curve are necessary to model wetting/drying cycles for a wide range of moisture content
- Considering film flow in hydraulic conductivity of soil plays a significant role to model wetting/drying cycles in low saturation degree

Correspondence to:
O. Ghasemi-Fare,
omid.ghasemifare@louisville.edu

Citation:
Tamizdoust, M. M., & Ghasemi-Fare, O. (2020). Utilization of nonequilibrium phase change approach to analyze the nonisothermal multiphase flow in shallow subsurface soils. *Water Resources Research*, *56*, e2020WR027381. https://doi.org/10.1029/2020WR027381

Received 21 FEB 2020
Accepted 29 JUL 2020
Accepted article online 4 AUG 2020

Abstract The prediction of coupled nonisothermal multiphase flow in porous media has been the subject of many theoretical and experimental studies in the past half a century. In particular, the evaporation phenomenon from the shallow subsurface has been extensively studied based on the notion of equilibrium phase change between liquid water and water vapor (i.e., instantaneous phase change). One of the frequent assumptions in equilibrium phase change approach is that liquid water is hydraulically connected throughout the vadose zone. Furthermore, classical soil-water retention curves (e.g., van Genuchten model), which have been extensively used in the literature to model evaporation process, are only valid for high and intermediate saturation degrees. Although these limitations have been addressed and improved in separate studies, they have not yet been rigorously incorporated in the numerical modeling of nonisothermal multiphase flow in shallow subsurface of in-field soils. Therefore, the aim of this study is to investigate the coupled heat, liquid, and vapor flow in soil media through the Hertz-Knudsen-Schrage (HKS) phase change model and by incorporating a water retention model which captures the soil-water characteristics from full to oven-dried saturation degrees. A numerical model is developed and validated against the in-field experimental data. Reasonable agreements between the calculated and measured values of water contents at all depths, as well as the temperature, and cumulative evaporation are observed. Results also confirm that the contribution of the film flow in overall mass flow in the medium is required for accurate modeling and cannot be ignored.

1. Introduction

Nonisothermal multiphase flow in porous media is the principal process involved in many engineering applications such as deep waste repositories, geothermal boreholes, buried high voltage cables (Hruška et al., 2019; Kroener et al., 2014; Moradi et al., 2016; Nguyen et al., 2017), and agricultural managements, for example, water availability prediction for the crops with respect to the uncertainties in climate change and variations of rainfall amounts and dry spell frequencies (Bittelli et al., 2008; Haghighi & Kirchner, 2017; Strati et al., 2018). Several experimental, theoretical, and numerical studies have been performed in the past decades to understand the coupled heat, liquid, and vapor flow and its impact on the temporal variations of temperature and moisture content of soils (Milly, 1982; Mohanty et al., 1998; Novak, 2010; Philip & De Vries, 1957; Saito et al., 2006).

One of the most important mechanisms concerning multiphase flow is the evaporation from the soil-atmosphere interface which plays a critical role in mass and energy exchange across this boundary (Brutsaert, 2015; Li et al., 2019). Two distinct stages of evaporation have been identified in the literature: Stage 1 of the evaporation starts at a high rate close to the saturated condition, and it is followed by a drastic decrease of the evaporation rate (i.e., falling rate) at which Stage 2 starts. Previous research demonstrated that the Stage 1 evaporation is controlled by the atmospheric demands where the capillary pressure delivers the pore water from the vadose zone to the soil surface. Stage 2 depends on hydraulic and thermal properties of the porous medium when a drying front is formed. The formation of the drying front in a deeper soil layer disrupts the liquid connection to the surface, and consequently, moisture transport occurs only in vapor diffusion (Or et al., 2013). Fick's law of diffusion is often used to calculate the vapor flow; however, according to the experimental evidence, it was found that Fick's law may underestimate vapor flow. Hence, the vapor diffusion enhancement factor was introduced first by Philip and De Vries (1957) to compensate for this underestimation (Cass et al., 1984).

Philip and De Vries (1957) proposed a theoretical model (PdV) to analyze the coupled heat, liquid, and vapor flow in porous media. PdV model has been used thereafter to predict the evaporation in soils (Novak, 2016). However, the validity of some of the assumptions made by Philip and De Vries (1957) has been questioned in recent years, such as the chemical and thermal equilibrium conditions (Niessner & Hassanizadeh, 2009b; Nuske et al., 2014; Ouedraogo et al., 2013; Smits et al., 2011) and vapor diffusion enhancement factor (Shokri et al., 2009). Shokri et al. (2009) argued the validity of vapor diffusion enhancement factor and stated that Fick's law can alone approximate vapor diffusion with the proper inclusion of capillary flow. Moreover, based on equilibrium phase change (EPC) assumption, it has been postulated that the timescale associated with the phase change (i.e., evaporation/condensation) in natural soils is shorter than the timescale of environmental forcing. Although, this assumption led to very important insights with less computational effort in modeling of the nonisothermal multiphase flow (by eliminating the need to calculate for water vapor density as an independent variable), it has been shown that the EPC assumption is not always valid (Benet et al., 2009; Chammari et al., 2003). Smits et al. (2011) conducted a numerical comparison between EPC and nonequilibrium phase change (NEPC) approaches and concluded that NEPC approach captured their laboratory-scaled experimental observation with better accuracy than the conventional EPC approach. Class et al. (2002) developed a numerical solution technique to simulate the nonisothermal multiphase and multicomponent processes (where fractions of different fluids may exist in liquid and/or gas phases simultaneously) based on the thermal and chemical equilibrium assumptions. The advantage of their model was to incorporate an adaptive switching of the primary variables upon the alteration of the thermodynamics state of the system (e.g., complete drying). Same concept is adapted in recent studies to model evaporation from soils by coupling free flow and porous medium flow (Fetzer et al., 2016; Mosthaf et al., 2011; Mosthaf et al., 2014). Nuske et al. (2014) extended the model proposed by Class et al. (2002) to include the effects of thermal and chemical nonequilibrium phenomena, where they concluded that considering chemical nonequilibrium (which may lead to NEPC) is of higher importance than the thermal nonequilibrium. Moreover, Massman (2015) studied the coupled mass and heat flow during wildfires considering a NEPC model. He proposed that the chemical potential of water cannot be in equilibrium with water vapor for soils closed to dry condition when almost no liquid water exists. Recently, Novak (2019) extended the PdV model with respect to NEPC approach to analyze the validity of NEPC from a steady-state simulation. His analysis showed, although NEPC is more likely to happen in coarse sands; however, it is negligible, and EPC assumption is still valid for most in-field evaporation processes. Assouline et al. (2013) observed an almost dry condition during Stage 2 of evaporation from a bare soil. They analyzed the dynamics of gravimetric water content obtained from the in-field soil samples and observed an almost dry condition for the subsurface soil. They mentioned that the numerical model, using HYDRUS-1D software which considers EPC assumption, could not predict the bare soil evaporation in which the hydraulic continuity is disrupted (Assouline et al., 2013; Assouline et al., 2014). Same conclusion was drawn by Dijkema et al. (2018) who measured the evaporation and analyzed heat and moisture distribution from desert sandy soil using a large weighing lysimeter.

Another important part of modeling of the nonisothermal multiphase flow is the soil-water retention (SWR) constitutive relation. Van Genuchten (1980) model (VG model) has been extensively used in literature. Saito et al. (2006) utilized the temperature-modified version of VG model to analyze the nonisothermal flow. Although this model was proved to be very accurate in capturing SWR behavior of different types of soil in capillary regime, it failed to predict the adsorption regime in which moisture content is below the residual water content (Zhang, 2011). Different SWR models have been proposed to account for adsorbed water behavior in almost dry condition (Or & Tuller, 1999; Revil & Lu, 2013).

Despite the several research studies over the years, predicting the evaporation rate and understanding the accurate moisture content for the in-field top soil are still challenging (Vanderborght et al., 2017). Recently, Gao et al. (2018) predicted the evaporation rate from soil subsurface observed in a controlled condition experiment by coupling free flow and mass transfer in porous media. Modeling free flow and mass transfer in porous media results in a realistic multiphysical interaction between different media (Fetzer et al., 2017). However, it should be noted that modeling of free flow under real-time meteorological conditions is complicated and has a high computational cost.

To the authors' knowledge, there are limited studies in the literature, which considered NEPC approach to simulate the evaporation from the field soil. Beyond this point, none of them could capture the dry zone during the bare soil evaporation. Therefore, the objective of this study is to analyze the nonisothermal

multiphase flow subjected to atmosphere evaporative demand where the evaporation rate at the soil-atmosphere boundary is scrutinized considering NEPC model and Fickian diffusion. We assume the validity of thermal equilibrium within the soil system, while NEPC is considered by utilizing the Hertz-Knudsen-Schrage (HKS) phase change model and incorporation of the liquid-gas interfacial area. In the present nonisothermal multiphase process, the gas phase may contain vapor and dry air where the dissolved gas in liquid phase is neglected for simplicity. Moreover, the generalized SWR model recently proposed by Lu (2016), which accounts for capillary and adsorption regimes, is modified to be temperature dependent and is used in the present analysis. First, details of the theoretical and numerical model are presented, and then, the performance of the model will be validated against the field measurement which was conducted at École polytechnique fédérale de Lausanne (EPFL) during the summer of 2006 using a weighable lysimeter filled with fine sand (Assouline et al., 2013). The simulated evaporation obtained by EPC model is also included for the sake of comparison with NEPC model.

2. Theoretical Formulation of Nonisothermal Multiphase Flow

The nonisothermal multiphase flow is composed of liquid and gas transport in advection and diffusion, and heat flow in convection and diffusion forms at macroscale. In this study, liquid refers to water, gas is the mixture of water vapor and dry air, and fluid includes liquid and gas where the dissolved gas in liquid is disregarded. Moreover, the phase change is assumed to only occur between liquid water and water vapor (i.e., evaporation/condensation). Hence, macroscopic mass balances of liquid and gas with balance of thermal energy are coupled and solved simultaneously. Furthermore, the phase change is governed by first-order macroscopic rate of kinetic mass transfer in porous media to consider NEPC. Here, a 1D model is used to reduce the computational cost. Therefore, all the formulations are presented along the z-axis of Cartesian coordinate system as follows.

2.1. Macroscopic Fluid Balance

The mass balances of liquid and gas phases can be written as (Bear, 2013):

$$\rho_l \frac{\partial \theta_l}{\partial \psi}\frac{\partial \psi}{\partial t} + \frac{\partial q_l}{\partial z} = -\dot{m}, \tag{1}$$

$$\rho_g \frac{\partial \theta_g}{\partial \psi}\frac{\partial \psi}{\partial t} + \frac{\partial q_g}{\partial z} = \dot{m}, \tag{2}$$

where θ_l and θ_g (m^3/m^3) are the volumetric contents of liquid and gas phases, respectively. ψ (Pa) is the matric suction and is defined as the difference between gas pressure (p_g) and pore liquid pressure (p_l) considering the force equilibrium between fluid phases ($\psi = p_g - p_l$). $\partial\theta_l/\partial\psi = -\partial\theta_g/\partial\psi$ is the moisture capacity and can be obtained from SWR constitutive relation. Please note that p_l and p_g are the primary variables in Equations 1 and 2 where the volumetric fluid contents (θ_l and θ_g) depend on suction potential through SWR curve. Moreover, $\dot{m}$ ($kg/m^3/s$) is the rate of NEPC; the positive and negative signs indicate condensation and evaporation, respectively, and will be discussed later.

The relationship between the volumetric liquid and gas contents is defined as $\theta_l + \theta_g = nS_l + nS_g = n(S_l + S_g)$, where n (m^3/m^3) is the porosity of the medium and S_l and S_g (−) are liquid and gas saturation degrees, respectively.

In Equations 1 and 2, q_l and q_g ($kg/m^2/s$) are the liquid and gas advective fluxes, respectively, and are expressed below:

$$q_l = \frac{\rho_l \kappa_{\text{int}} \kappa_{rl}}{\mu_l}\frac{\partial}{\partial z}(p_l + \rho_l g z), \tag{3a}$$

$$q_g = \frac{\rho_g \kappa_{\text{int}} \kappa_{rg}}{\mu_g}\frac{\partial}{\partial z}\left(p_g + \rho_g g z\right), \tag{3b}$$

where κ_{int} (m^2) is the intrinsic permeability of the medium. κ_{rl} and κ_{rg} (−) are the relative permeabilities of liquid and gas phases; μ_l and μ_g (Pa·s) are dynamic viscosities of liquid and gas, respectively, and g (m/s^2)

is acceleration of gravity. ρ_l (kg/m^3) is the density of the liquid, and ρ_g (kg/m^3) is the density of gas. The density of gas can be written as the summation of dry air and water vapor densities in which both are governed by the ideal gas law. Lu and Likos (2004) derived Equation 4 by considering that dry air pressure is equal to the difference of atmospheric pressure (p_a) and the vapor pressure (p_v):

$$\rho_g = \frac{p_a M_a}{RT} - \left(\frac{M_a}{M_w} - 1\right)\rho_v, \tag{4}$$

where R (Pa·m^3/K/mol) is the universal gas constant, M_w and M_a (kg/mol) are the molecular weight of liquid and dry air, respectively. T (K) is the temperature, and ρ_v (kg/m^3) is the vapor density.

2.2. Soil-Water Retention Characteristics

In order to analyze the unsaturated flow in soil media, a constitutive relationship (SWR model) must be defined between the matric suction and volumetric liquid content. There are several SWR models available in literature which predict the capillary range of soil-water characteristics with enough accuracy. Among those, Lu (2016) proposed an SWR model which accounts for capillary and adsorptive regimes distinctively from high to low matric potentials (i.e., matric suction) and is presented below. The first step is the decomposition of the volumetric liquid content into the capillary and adsorbed liquid:

$$\theta_l(\psi) = \theta_a(\psi) + \theta_c(\psi). \tag{5}$$

In Equation 5, θ_a and θ_c are the volumetric contents corresponding to the adsorption and capillary regimes. The adsorption volumetric liquid content is formulated as follows:

$$\theta_a(\psi) = \theta_{a,\,\max}(T)\left\{1 - \left[\exp\left(\frac{\psi - \psi_{\max}}{\psi}\right)^M\right]\right\}. \tag{6}$$

In Equation 6, $\psi_{\max}$ (Pa) is the highest suction at which volumetric liquid content reaches zero and M is adsorption strength ($0 < M < 1$). Clayey soils have higher adsorption capacity as they can retain more water, and therefore, adsorption occurs for suctions in the order of several hundreds of megapascals. On the contrary, sandy soils have less adsorption capacity, and it can be triggered for suctions in the order of several thousands of kilopascals. Moreover, $\theta_{a,\max}$ is the maximum adsorption capacity which can be interpreted as the residual liquid content commonly used in SWR models. In this study, the maximum adsorption capacity in the SWR model is defined as: $\theta_{a,\max}(T) = \theta_{a,\max}(T_{ref})[1-c(T-T_{ref})]$. This definition is the temperature-dependent form of the residual liquid content which was proposed by She and Sleep (1998), where T_{ref} (K) is the reference temperature and c (−) is a fitting parameter.

For capillary regime, Lu (2016) proposed a modification for volumetric liquid content with respect to the water cavitation which involves metastable phase change (Herbert et al., 2006). This modification is considered as a normal distribution function imposed on VG model as follows:

$$\theta_c\psi = \frac{1}{2}\left[1 - \mathrm{erf}\frac{\psi - \psi_{\mathrm{cav}}}{\sqrt{2}\sigma_{\mathrm{cav}}}\right][n - \theta_a\psi][1 + |\alpha\psi T|^{n_{VG}}]^{-m_{VG}}, \tag{7}$$

where erf() is the error function; ψ_{cav} (Pa) is the mean cavitation suction; and σ_{cav} (Pa) is the standard deviation, and it is equal to $0.4\psi_{\mathrm{cav}}$ in this study. α (1/Pa), n_{VG}, and $m_{VG} = 1–1/n_{VG}$ are VG model parameters. $\psi(T)$ is defined by Grant and Salehzadeh (1996): $\psi(T) = [\sigma(T_{ref})/\sigma(T)]\,\psi(T_{ref})$. In which, σ (Pa/m) is the surface tension. Equations 5, 6, and 7 define a general form of the SWR characteristic with seven isothermal and two nonisothermal parameters. The presented SWR model serves a significant role in modeling of evaporation from soils close to dry state and is implemented in the numerical model presented in this study.

In unsaturated flow, the film flow may have an important contribution to the overall hydraulic conductivity of a medium when the soil dries out (Smits et al., 2012). Generally, hydraulic conductivity of the saturated soil can be presented as the decomposition of hydraulic conductivity due to the capillary flow, k_{cap} (m/s) and the film flow, k_{film} (m/s). k_{cap} was described by Van Genuchten (1980): $k_{\mathrm{cap}} = k_s\kappa_{rl}$, where k_s (m/s) is

the saturated hydraulic conductivity. The model for hydraulic conductivity due to film flow is adapted from Zhang (2011), which is a modification of the original model proposed by Tokunaga (2009):

$$k_{\text{film}} = f(1-n)\frac{\sqrt{2d_g}\pi^2\rho_l g}{\mu_l}\left(\frac{\varepsilon\varepsilon_0}{2\sigma}\right)^{1.5}\left(\frac{k_b T}{z_i a}\right)^3\left(1+\frac{d_g\psi}{2\sigma}\right)^{-1.5}, \tag{8}$$

where f is the dimensionless correction factor, d_g (m) is the effective grain diameter, $\varepsilon = 78.54$ is the dimensionless relative permittivity of water, $\varepsilon_0 = 8.85\times10^{-12}$ (C^2/J/m) is permittivity of free space, $k_b = 1.381\times10^{-23}$ (J/K) is the Boltzmann constant, z_i is the dimensionless magnitude of the ionic charge and is assumed to be equal to 1, and $a = 1.602\times10^{-19}$ (C) is the electron charge. The $f = 1$ correction factor in Equation 8 accounts for the nonuniformity of the porous media, that is, represents smooth uniform spherical grains. Smits et al. (2012) and Massman (2015) considered the film flow according to Equation 8 in their models and acknowledged the importance of considering the hydraulic conductivity due to the film flow for dry state conditions. But they found no improvement in the numerical results. However, during soil evaporation, when soil moisture content reaches below residual moisture content, the matric suction increases drastically to a limiting value of oven-dried suction (also known as $\psi_{\max}$). In this condition, the capillary liquid conductivity will be disrupted, and liquid mass transfer will be carried out by the film flow. Therefore, including film flow in numerical modeling provides a continuous diffusivity of the high suction gradient with respect to the wetting/drying dynamic cycles in soils and improves the overall convergence of the model. Consequently, the inclusion of film flow in hydraulic conductivity seems necessary to model the nonisothermal multiphase flow.

2.3. Vapor Transport

In NEPC approach, vapor density (ρ_v) is an independent variable, and it needs to be coupled with the mass balance equations of liquid and gas as follows:

$$\frac{\partial}{\partial t}(\theta_g\rho_v) + \frac{\partial}{\partial z}\left(\rho_v u_g - D_v\frac{\partial\rho_v}{\partial z}\right) = \dot{m}. \tag{9}$$

$u_g = q_g/\rho_g$ is the advective gas velocity. D_v (m^2/s) is the effective diffusivity ($D_v = \tau\theta_g D_v^{\,0}$, τ is tortuosity, and $D_v^{\,0}$ (m^2/s) is the binary diffusion coefficient of vapor in gas phase). The vapor diffusion is considered according to the Fick's first law of diffusion. Note that, unlike many nonisothermal multiphase flow models, the enhancement factor does not need to be considered in the formulation of effective diffusivity. Please also note, the definition of vapor density in Equation 9 deviates from its definition in EPC approach which states that the vapor density is always equal to its saturated state according to Kelvin's law (Milly, 1982).

2.4. Macroscopic Energy Balance

For nonisothermal flow, Equation 10 presents the heat balance equation (Whitaker, 1977):

$$(\rho C)_m\frac{\partial T}{\partial t} + \frac{\partial}{\partial z}\left[\left(\rho_l u_l C_l + \rho_g u_g C_g\right)T - \lambda_m\frac{\partial T}{\partial z}\right] = -L_v\dot{m}. \tag{10}$$

$u_l = q_l/\rho_l$ is the advective liquid velocity. ρ_m (kg/m^3), C_m (J/kg/K), and λ_m (W/m^2/K) are the effective density, specific heat capacity, and thermal conductivity of the medium, respectively. C_l and C_g are the specific heat capacities of liquid and gas phases, respectively. L_v (J/kg) is the latent heat of vaporization. The presented multiphase flow model assumes the local thermal equilibrium among all the phases (i.e., $T_l = T_g = T_s = T$).

2.5. Nonequilibrium Phase Change

In porous media, NEPC is controlled by the first-order rate of kinetic mass transfer between fluid phases (liquid water and water vapor), and it governs the difference between the actual and equilibrium vapor densities (Niessner & Hassanizadeh, 2009a):

$$\dot{m} = a_{lg}\kappa_{lg}\left(\rho_{v,\,eq} - \rho_v\right). \tag{11}$$

a_{lg} (1/m) is the volume-normalized liquid-gas interfacial area, κ_{lg} (m/s) is the mass transfer rate coefficient, and $\rho_{v,eq}$ (kg/m^3) is the equilibrium vapor density. According to Kelvin's law, relative humidity can be related to the matric suction as follows: $RH = \rho_v/\rho_{v,sat} = \exp[\psi M_w/(RT\rho_l)]$, where $\rho_{v,sat}$ (kg/m^3) is the saturated vapor density. Please note that in case of EPC condition, vapor density and equilibrium vapor density are identical ($\rho_{v,eq=}\rho_v$).

Different NEPC models have been proposed based on Equation 11 in the literature. Trautz et al. (2015) preformed a numerical comparison among these models and compared the results with the experimental observation of the bare soil evaporation. In this study, the HKS model is employed, which is a modification of Hertz-Knudsen (HK) model of evaporation and condensation. The advantage of the HKS model was verified in the literature through different nonisothermal multiphase analyses of the evaporation process (Massman, 2015; Trautz et al., 2015). The HKS model is derived based on the kinetic theory of gases as follows (Kryukov & Levashov, 2011):

$$\dot{m} = \theta_l a_{lg}\frac{1}{1 - 0.5f_c}\sqrt{\frac{RT}{2\pi M_w}}\left(f_e\rho_{v,\,eq} - f_c\rho_v\right), \tag{12}$$

where $[1/(1-0.5f_c)]\sqrt{RT/(2\pi M_w)}$ is the mass transfer rate coefficient (κ_{lg}). The volumetric liquid content is included to express the phase change reaction in terms of mass per unit volume of soil per time (Trautz et al., 2015). Furthermore, f_e and f_c (−) are the evaporation and condensation coefficients. f_e is the ratio of number of molecules transferred to the vapor phase to the total number of molecules emitted from the liquid phase. In analogy, f_c is the ratio of the number of molecules adsorbed by the liquid phase to the total number of molecules impinging on the liquid phase (Marek & Straub, 2001). Despite their physical meaning, evaporation and condensation coefficients are very hard to determine, and there is still ongoing theoretical and experimental research to obtain these values (Jafari et al., 2018). Both f_e and f_c values for water have been observed to vary from 10^{-4} to 1, and also, they are not necessarily identical: $f_e \neq f_c$ (Marek & Straub, 2001). Recently, Persad and Ward (2016) conducted an extensive review on theoretical, experimental, and molecular dynamics studies of evaporation and found out that both coefficients are not always less than unity. It is evident that both f_e and f_c are functions of liquid and vapor temperature, heat flux, and geometry (Jafari et al., 2018). In the literature, f_e and f_c are often considered according to the Arrhenius equation by using the surface condensation/evaporation activation energy (Vlasov, 2019). In this study, the evaporation and condensation coefficients are assumed to be constant and are calibrated with respect to the accumulative evaporation data which are the same as the procedure performed by Trautz et al. (2015).

The liquid-gas interfacial area (a_{lg}) can be determined experimentally (Araújo & Brusseau, 2019; Peng & Brusseau, 2005) or through the pore scale modeling (Jiang et al., 2020; Joekar-Niasar et al., 2008; Nuske et al., 2014). The liquid-gas interfacial area is a function of liquid saturation degree (S_l) and is equal to zero when $S_l = \{0 \text{ or } 1\}$. In addition, the experimental observation showed that the liquid-gas interfacial area reaches its maximum value at a low saturation degree for sands (Costanza-Robinson & Brusseau, 2002). Since there is limited research on predicting the interfacial area, a parabolic function proposed by Costanza-Robinson and Brusseau (2002) and Massman (2015) is used in this study with a slight modification:

$$a_{lg} = \alpha_1 S_l(1 - S_l)^{\alpha_2} + \alpha_3[S_l(1 - S_l)]^{\alpha_4}. \tag{13}$$

$\alpha_1 = 50$, $\alpha_2 = 20$, $\alpha_3 = 0.22$, and $\alpha_4 = 0.25$ are fitting parameters. Considering Equation 13 and the fitting parameters, the interfacial area reaches its maximum value at $S_l = 1\%$. Please note, for more accurate elucidation of the interfacial area in Equation 13, the specific surface area of the soil should be measured. Nonetheless, the presented interfacial area (Equation 13) represents our current understanding of interphase between bulk liquid and gas phases in full range of the saturation degree. Bulk liquid refers to the state when liquid is in capillary regime; therefore, when liquid is adsorbed as film regions on soil particles, the phase change does not take place.

Table 1
The Dependent Parameters Used in the Nonisothermal Multiphase Flow Equations

Parameter	Equation
Liquid density (Hillel, 2013)	$\rho_l = 1 - 7.37 \times 10^{-6}(T-4)^2 + 3.79 \times 10^{-8}(T-4)^3$
Relative permeability of liquid (Van Genuchten, 1980)	$\kappa_{rl} = S_{eff}^{0.5}\left[1 - \left(1 - S_{eff}^{\frac{1}{m_{VG}}}\right)^{n_{VG}}\right]^2$[a]
Relative permeability of gas (Van Genuchten, 1980)	$\kappa_{rg} = \left(1 - S_{eff}\right)^{0.5}\left(1 - S_{eff}^{\frac{1}{m_{VG}}}\right)^2$
Saturated vapor density (Bittelli et al., 2015)	$\rho_{v,sat} = 0.001T^{-1}\exp(31.37 - 6014.79T^{-1} - 0.00792T)$
Binary vapor diffusion coefficient (Bittelli et al., 2015)	$D_v^0 = 2.92 \times 10^{-5}(T/273.15)^2$
Tortuosity (Millington & Quirk, 1961)	$\tau = n^{-2}\theta_g^{7/3}$
Surface tension (Grant & Salehzadeh, 1996)	$\sigma = 0.1177 - 0.0001535\ \mathrm{T}$
Latent heat of vaporization (Monteith & Unsworth, 2013)	$L_v = 2.501 \times 10^6 - 2369.2(T + 273.15)$
Thermal conductivity of the medium (Bittelli et al., 2015; Campbell et al., 1994)	$\lambda_m = \frac{k_l\theta_l\lambda_l + k_g\theta_g\lambda_g + k_s 1 - n\lambda_s}{k_l\theta_l + k_g\theta_g + k_s 1 - n}$

[a] $S_{eff} = (\theta_l - \theta_a)/(n - \theta_a)$ is the effective liquid saturation degree.

All the temperature-dependent and saturation-dependent parameters used in Equations 1 to 13 are presented in Table 1. The rest of parameters are calculated from the formulations provided by the International Association for the Properties of Water and Steam (IAPWS 2007) (Tamizdoust & Ghasemi-Fare, 2020; Wagner & Kretzschmar, 2008). In Table 1, the thermal conductivity of the medium depends on the volumetric liquid content, temperature, and clay fraction on the medium according to Bittelli et al. (2015), and it has been incorporated in different numerical models to predict the nonisothermal evaporation process (Bittelli et al., 2008; Kroener et al., 2014; Trautz et al., 2015). Figure 1 illustrates the thermal conductivity of the medium with respect to the volumetric liquid content at different temperatures.

2.6. Equilibrium Phase Change Formulation

EPC formulation can be retrieved by combining liquid mass balance (Equation 1) and vapor transport (Equation 9), which eliminates the phase change source term. In EPC approach, the gas pressure is assumed to be constant in time and space and is equal to atmospheric pressure. Moreover, as stated before, the vapor density is not an independent variable and is equal to its equilibrium value, that is, $\rho_{v,eq} = \rho_v$. Furthermore, in the energy balance equation (EBE), the time variations of equilibrium vapor density and its diffusion in space are considered as the latent heat source term:

$$\rho_l \frac{\partial \theta_l}{\partial \psi}\frac{\partial \psi}{\partial t} + \frac{\partial}{\partial z}\left(q_l - D_v \frac{\partial \rho_{v,eq}}{\partial z}\right) = 0, \tag{14}$$

$$(\rho C)_m \frac{\partial T}{\partial t} + \frac{\partial}{\partial z}\left[(\rho_l u_l C_l)T - \lambda_m \frac{\partial T}{\partial z}\right] = -L_v\left[\frac{\partial}{\partial t}\left(\theta_g \rho_{v,eq}\right) - \frac{\partial}{\partial z}\left(D_v \frac{\partial \rho_{v,eq}}{\partial z}\right)\right]. \tag{15}$$

In Equation 14, the variations of equilibrium vapor density with time are disregarded with respect to time variations of matric suction. The independent variables in EPC approach are matric suction (ψ) and temperature (T). Moreover, same as in NEPC approach, no enhancement factor is considered for the vapor diffusion. The results of NEPC modeling approach (Equations 1, 2, 9, and 10) and EPC modeling approach (Equations 14 and 15) will be compared later in the numerical study.

In addition to general heat, liquid, and gas flow in porous media, atmospheric boundary conditions must be carefully defined to accurately model the bare soil evaporation.

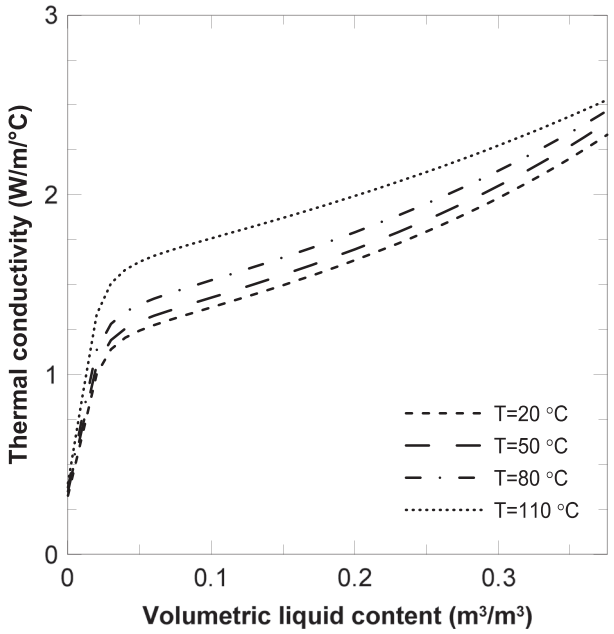

Figure 1. Thermal conductivity of the medium.

2.7. Vapor Transport Boundary Condition

Vapor flux, E (kg/m^2/s), from the soil-atmosphere boundary, can be described using the difference between the vapor density at the soil surface and the equilibrium vapor density of air, $(\rho_{v,eq})_a$ (kg/m^3), at a reference height, z_{ref} (m), and equivalent aerodynamic resistant coefficient to mass transfer, r_v (s/m):

$$E = \frac{1}{r_v}\left[\rho_v - \left(\rho_{v,\,eq}\right)_a\right]. \tag{16}$$

r_v can be calculated from the explicit approach adapted in Choudhury et al. (1986) and Sviercoski et al. (2018):

$$r_v = \frac{1}{\kappa^2 \upsilon}\left(\log\frac{z_{ref}}{z_0}\right)^2 (1+\delta)^{\nu}, \tag{17a}$$

$$\delta = 5g\frac{(z_{ref}-d)(T-T_a)}{T_a \upsilon^2}, \tag{17b}$$

$$\nu = \begin{cases} -2 & \delta < 0 \\ -0.75 & \delta > 0 \end{cases}. \tag{17c}$$

δ (−) is the atmospheric stability factor, υ (m/s) and T_a (K) are the wind speed and air temperature recorded at the local station at the z_{ref} (m) height, $\kappa = 0.41$ (−) is the von Karman constant, z_0 (m) is the surface roughness, and d (m) is a constant parameter. The value of d is zero for soils with no vegetation. Equation 17a yields an exact solution for atmospheric stable conditions and an approximate value for unstable conditions with a reasonable accuracy (Choudhury et al., 1986). Note that $1/r_v$ serves as a vapor mass transfer coefficient.

Different attempts have been made in the literature to modify the vapor mass transfer coefficient by including a vapor resistivity parameter in dry layers. van de Griend and Owe (1994) proposed an empirical equation to predict the soil vapor diffusivity resistance which is frequently used in the bare soil evaporation (Bittelli et al., 2008; Smits et al., 2011). In this approach, the value of liquid water content at the top 1 cm is required. Another approach was proposed by Shokri et al. (2009) to directly estimate the evaporation rate from the soil by utilizing the Fick's law for the shallow depth of the drying layer. This approach is based on the knowledge of the dry layer thickness which can be difficult to determine for field conditions (Smits et al., 2012).

Combining Equations 16 and 17a–17c is the simplest form of the vapor flux from soil-atmosphere boundary which controls the upper boundary condition of vapor transport (Equation 9) in case of NEPC approach, or liquid water and vapor transport (Equation 14) in case of EPC approach. As it will be seen later, Equation 16 can adequately predict the evaporation rate using the presented nonequilibrium model in comparison to the equilibrium model. Furthermore, the aerodynamic resistant coefficient remains the sole transfer coefficient to couple the atmospheric condition with the shallow subsurface flow.

2.8. Energy Balance Equation

In case of the evaporation across the soil-atmosphere boundary, a coupled energy exchange between porous media and free flow should be established (Brutsaert, 2005). In the literature, it is suggested that a boundary layer may exist above the soil surface for the momentum, mass, and energy transport. Although the existence of the boundary layer alone may not accurately represent the actual in-field condition (Vanderborght et al., 2017), however, it can be used as a suitable approximation instead of coupling free flow and flow in porous media. Hence, EBE in the boundary layer is described as:

$$G = R_n - H - L_v E. \tag{18}$$

G, R_n, and H (W/m^2) are the surface, net solar radiation, and sensible heat flux from the top boundary, respectively, and L_vE is the latent heat of evaporation. On the right-hand side of the Equation 18, the positive sign represents the incoming fluxes towards the soil surface and the negative signs demonstrate the outgoing flux.

Table 2
Hydraulic Properties of Fine Sand and Shonai Dune Sand

Soil	n (m^3/m^3)	$\theta_{a,max}$ (m^3/m^3)	K_s (m/h)	n_{VG} (−)	α (1/m)	c (−)	ψ_{cav} (MPa)	ψ_{max} (MPa)	M (−)	f (−)	d_g[a] (mm)	f_e (−)	f_c (−)
Fine sand	0.376	0.02	0.791	2.15	8.3	0.015	15	300	0.005	50	0.17	0.06	0.065
Shonai dune sand	0.43	0.044	0.360	4.95	4.07	N/A[b]	15	300	0.005	N/A	N/A	N/A	N/A

[a]Estimated based on hydraulic conductivity (K_s) using Kozeny–Carman model (Chapuis & Aubertin, 2003). [b]Not applied.

The solar radiation is composed of net shortwave (R_{ns}) and longwave (R_{nl}) radiations as follows:

$$R_n = R_{ns} + R_{nl} = (1 - \alpha_{alb})S_n + \varepsilon_s\sigma_s\left\{\left[(1 - 0.84c_f)\varepsilon_a + 0.84c_f\right]T_a{}^4 - T^4\right\}. \quad (19)$$

When the sky is cloudy, the atmospheric emissivity is defined as $[(1 - 0.84c_f)\varepsilon_a + 0.84c_f]$ (Monteith & Unsworth, 2013), where c_f is the cloud factor. In Equation 19, S_n (W/m^2) is the incoming solar radiation obtained from meteorological data. α_{alb} and ε_s are surface albedo and soil surface emissivity, respectively, and $\sigma_s = 5.67 \times 10^{-8}$ ($W/m^2/K^4$) is the Stefan–Boltzmann constant (Bittelli et al., 2015). Calculations of surface albedo, soil surface emissivity, and air emissivity are given in Appendix A.

The sensible heat flux due to convection is given by

$$H = \frac{C_v}{r_H}(T - T_a). \quad (20)$$

C_v (=1,200 $J/m^3/K$) is the volumetric heat capacity of the air, and r_H (s/m) is the aerodynamic resistance to heat transfer and is assumed to be equal to r_v.

The evaporation across the soil-atmospheric boundary and the heat, liquid, and gas flow in soil media can be predicted by coupling the balance of fluid and heat with vapor transport equations considering the EBE boundary equation in a finite element numerical model. Hence, the developed model is used to analyze the evaporation in a field condition considering temperature-modified Lu and VG models and NEPC and EPC approaches.

3. In-field Experiment and Numerical Simulation Descriptions

3.1. Description of the Field Experiment

In order to evaluate the capability of the theoretical model presented above, the evaporation from a bare soil is simulated in this study. The experiment was performed at the EPFL in the summer of 2006 from June 29 to July 3 for 120 h (Assouline et al., 2013). A cylindrical weighable lysimeter as a polyester reinforced fiberglass tank was placed below the ground in which the surface of the tank was exposed to the natural atmospheric condition. The tank was filled mostly with local fine sand which contained 98% sand, 1% silt, and 1% clay. Tensiometer and thermocouple sensors were embedded to measure the capillary head and the temperature at different depths. The experiment was carried out staring with saturating the soil from the bottom of the tank and then lowering the water table to the depth of $z = -80$ cm before the beginning of the experiment. The experiment was executed under the atmospheric forcing according to the climatic data from a micrometeorological station located 10 m away from the site. The micrometeorological data and more details on the lysimeter experimental procedure are available in Assouline et al. (2013). Please see Appendix B for more details.

The hydraulic properties used in the numerical model are borrowed from the field measurements and are presented in Table 2. However, prior to the multiphasic numerical modeling, the SWR model proposed by Lu (2016) and Van Genuchten (1980) are compared with the experimental measurement from the under study sand and another similar sandy soil called "Shonai dune sand" (93.3% sand, 1% silt, and 5.7% clay) (Mehta et al., 1994) which are presented in Figures 2a and 2b, respectively. The mean cavitation and maximum pressure as well as the adsorption strength in the SWR model (Equation 7) are determined with respect to fitting procedure with the SWR experimental data for Shonai dune sand. As it can be seen in Figure 2b, Lu's model captures the SWR characteristics of Shonai dune sand reasonably well for low liquid

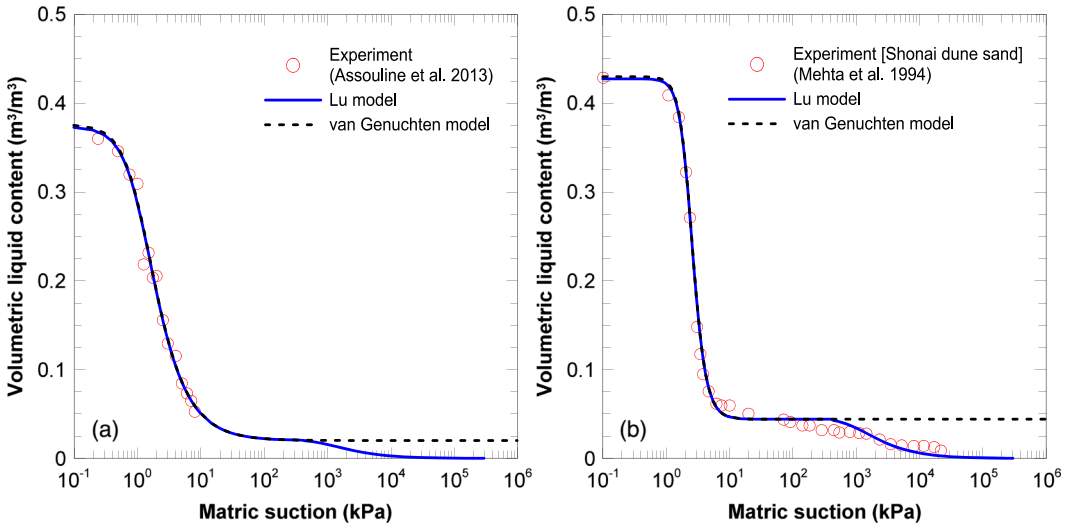

Figure 2. Comparison of Lu (2016) water retention curve used in this study and VG model with the experimental data of (a) fine sand and (b) Shonai dune sand.

volumetric content. Comparably, same fitting parameters for mean cavitation, maximum pressure, and adsorption strength are used for the fine sand in this study.

3.2. Description of the Numerical Model

A finite element numerical model is adapted to solve the set of highly nonlinear equations described in the previous section using COMSOL Multiphysics software v5.3a. The initial and boundary conditions are explained below.

According to the field condition, the water table is initially considered at $z = -80$ cm to calculate hydrostatic pore liquid pressure. In both EPC and NEPC modeling approaches, no-flux boundary condition is assumed for liquid flow in bottom boundary. Moreover, the initial temperature for the soil domain and the bottom boundary is considered as 23°C based on the field measurement. The EBE equation is assigned for the top boundary for Equations 10 and 15 to consider the heat transfer across the land-atmosphere interface according. In EPC model, the evaporation rate (Equation 16) governs the top boundary condition for liquid and vapor flow (Equation 15). In NEPC model, the initial and top boundary conditions for gas pressure are assigned to be equal to atmospheric pressure, and no gas flow boundary is assumed for the bottom boundary. Initial vapor density is assumed to be equal to its equilibrium value. Since the evaporation is happening from the soil surface, the time-dependent vapor transport from top boundary is also considered according to the Equation 16. Vapor density gradient with respect to z-axis in bottom boundary is set to zero (i.e., no flow).

The length of the subsurface soil is 100 cm, and after mesh sensitivity analysis, the domain is discretized with 200 two-noded beam elements. The model is solved using the PARADISO direct matrix solver built in COMSOL Multiphysics. The relative tolerance for the nonlinear analysis is set to 0.001.

4. Numerical Results and Interpretation of the Data

Figures 3a and 3b present the variations of volumetric liquid content and temperature of the soil medium at different depths and compare the numerical (NEPC approach) and experimental results. In general, volumetric liquid contents obtained from the numerical model match with experimental observations at all three depths. Please note that the experimental data were obtained from the tensiometers and the volumetric liquid contents were calculated based on the VG model; however, according to the Figure 2, both Lu and VG models coincide for liquid water contents higher than the maximum residual liquid content. Therefore, same liquid water contents reported in Assouline et al. (2013) are used for validation of the current simulation. Please note, for any liquid water content below the residual value, this comparison will have some discrepancy unless liquid water contents are measured directly. The nonisothermal diurnal fluctuations of volumetric liquid contents due to variations in atmospheric conditions follow the same trend as

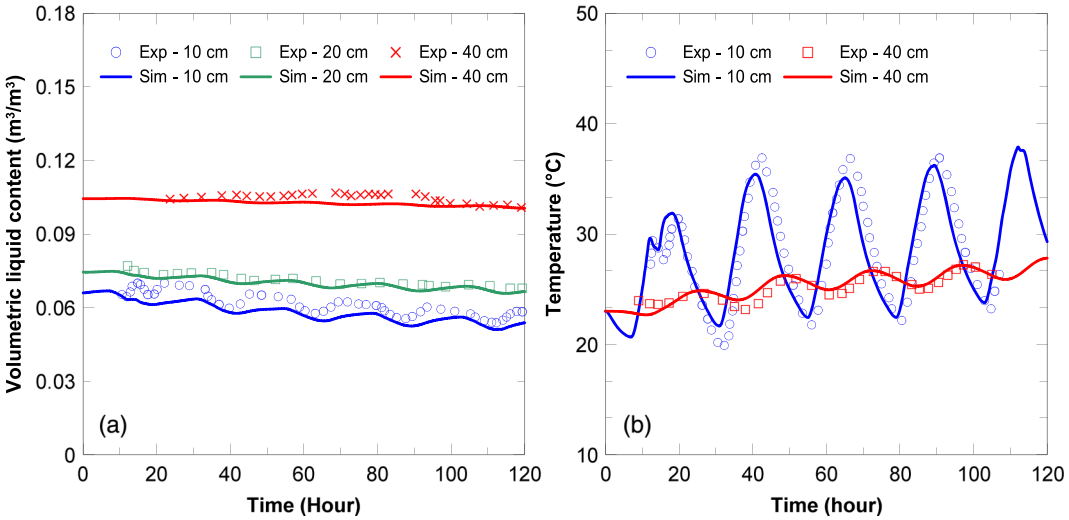

Figure 3. Simulated variations of (a) volumetric liquid content and (b) temperature at different depths considering NEPC approach with comparison to the experimental observations (Assouline et al., 2013).

were observed in the field with a minor underestimation at $z = -10$ cm. The results of simulated liquid volumetric content obtained in this study are improved compared to the original numerical study performed by Assouline et al. (2013) in which the pattern of the fluctuations could not be captured. It is interesting to note that, considering the pore liquid and gas pressures as primary variables in Equations 1 and 2, instead of using volumetric liquid and gas contents, improves the results. Furthermore, using the temperature-dependent maximum adsorption capacity in SWR model controls the magnitude of diurnal fluctuations of volumetric liquid content. Moreover, the simulated temperature variations at different depths match well with the field observations (Figure 2b).

Figures 4a and 4b show the measured and simulated cumulative evaporation for the 5 days and for the last day of the experiment, respectively. The simulations carried out considering both NEPC and EPC approaches. Furthermore, temperature-modified Lu model is compared with the VG model to better perceive the effect of SWR models on evaporation dynamics in soils. Figure 4a confirms the accuracy of NEPC model

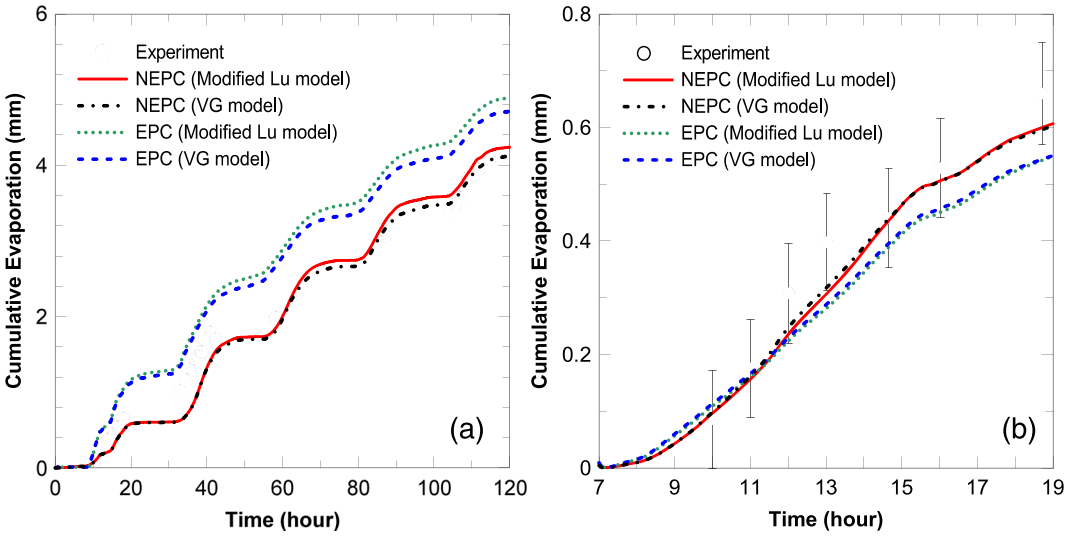

Figure 4. Simulated cumulative evaporation with comparison to experimental observations (Assouline et al., 2013): (a) for 5 days of the experiment and (b) last day of the experiment.

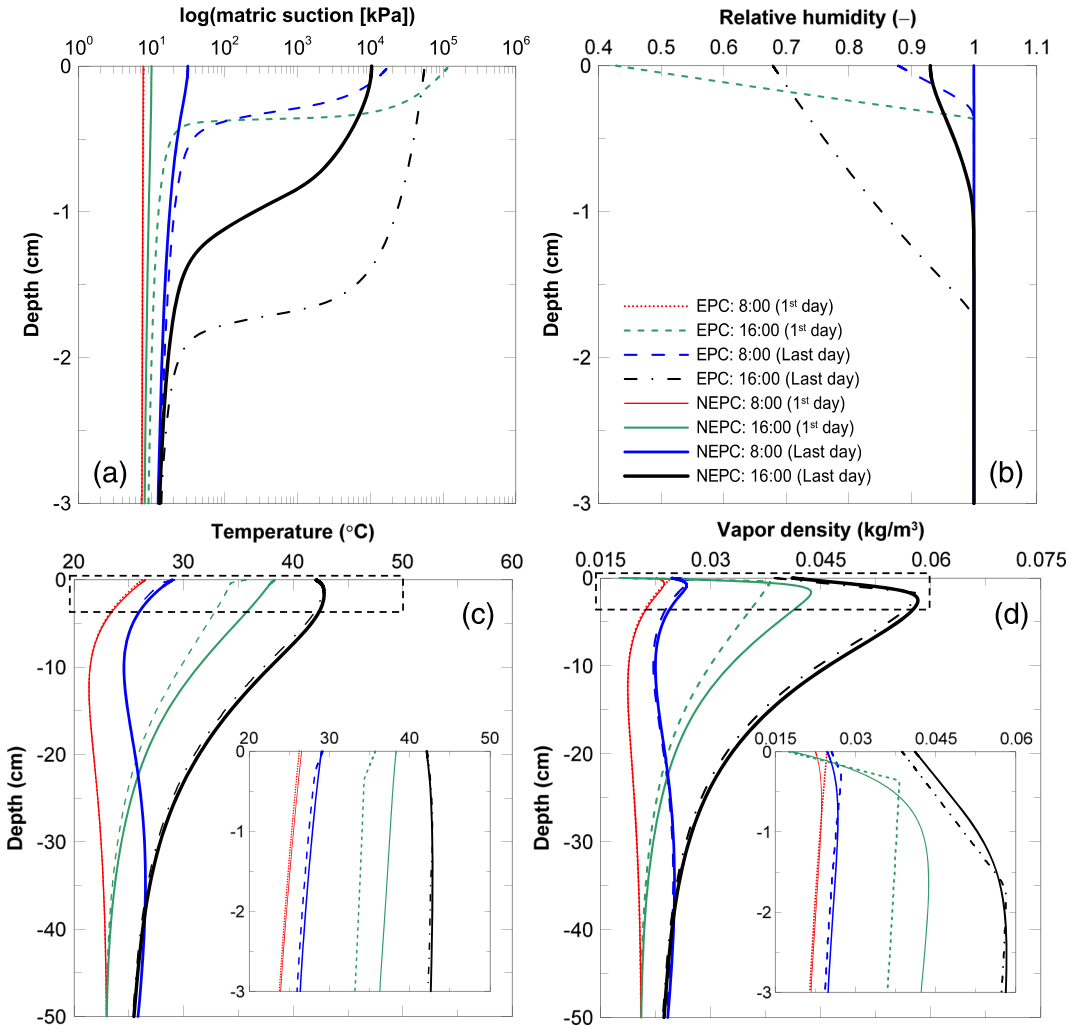

Figure 5. The simulated (a) matric suction, (b) relative humidity, (c) temperature, and (d) vapor density for two different hours of the first and last day of the experiment with EPC and NEPC approaches.

which can predict the cumulative evaporation as observed in the field, while EPC model overestimates the cumulative evaporation during the time of the experiment. In both EPC and NEPC approaches, the VG model's predictions are slightly lower than the temperature-modified Lu model which stem from the fact that VG model allows no further liquid reduction from the soil system when it reaches to its residual value; however, this limitation has been relaxed in Lu model. In Figure 4b, the changes in cumulative evaporation are illustrated which were measured from early in the morning (7:00) to the evening (19:00) on the last day. The predicted cumulative evaporation with NEPC model matches well with the experimental data, while EPC model underestimates the last day's cumulative evaporation. The underestimation of cumulative evaporation in the last day of experiment is because of the higher evaporation rate predicted by EPC approach in the first 2 days of the experiment. In EPC model, the liquid water content has already been evaporated from the shallow subsurface soil, and there is extensively lower liquid water for phase change and evaporation for the last day. Moreover, as it can be seen in Figure 4b, both Lu and VG models yield almost the same result in both EPC and NEPC modeling approaches.

Assouline et al. (2013) simulated the cumulative evaporation of the last day using the equation originally proposed by Shokri et al. (2009) which is based on Fickian vapor diffusion and considering the thickness of dry soil layer. They measured the thickness of dry soil layer from the gravimetric liquid content profile of the top layer of soil obtained from destructive sampling (the experimental data are available in

Figure 8). They concluded that the model proposed by Shokri et al. (2009) underestimates the cumulative evaporation of the last day. Therefore, they suggested an additional advective vapor transfer equation to account for the evaporation that happens in the morning with respect to the atmospheric evaporative demand. In this study, the evaporation and condensation processes are carefully accounted through NEPC approach. As it was mentioned earlier, nonequilibrium model relaxes the equilibrium assumption where the vapor density does not have to be equal to its equilibrium value. Figure 4b indicates the fact that the evaporation flux can be governed by Fickian diffusion if the actual vapor density is calculated by NEPC model and is employed in Equations 16 and 18.

To further investigate the effect of NEPC approach on the evaporation process, the dynamics of matric suction, relative humidity, temperature, and vapor density are shown in Figures 5a–5d for the first and last day of the experiment in the morning (8:00) and in the afternoon (16:00). For the sake of comparison, the results of EPC approach using same SWR model (Lu model) are also included in Figure 5. Figure 5 compares the different dynamics of thermal and hydraulic behavior of the soil in the vicinity of the natural evaporative boundary obtained from EPC and NEPC approaches. These differences result in deviation of actual and equilibrium vapor densities in the soil.

Figure 5a shows minimal changes in matric suction for the first day of the experiment simulated by NEPC model, which implies that the atmospheric demand has a little effect on the initially hydrostatic condition of the soil during the first day. EPC model predicts same type of behavior in the morning; however, in the afternoon (at 16:00), much higher suction is evident in the top 0.5 cm of the soil in comparison to NEPC model. Moreover, intense changes in matric suction from early morning to the afternoon are evident in the last day. This fluctuation occurs due to the hourly variations of atmospheric conditions and relatively dryer soil layer in comparison to the first day. According to EPC modeling approach, the influential zone of high matric suction is about 2 cm below the ground in the afternoon while it is controlled by the capillary suction in deeper soil layers. The influential zone of high matric suction calculated by NEPC model is about 1.5 cm below the ground for the same time. As it can be seen from Figure 5a, EPC model predicts much higher matric suction day than NEPC model (except only for the morning of the first day). It should be mentioned that Smits et al. (2011) and Li et al. (2019) also concluded that EPC model predicted a very high and sudden jump in the matric suction when soil dries out which, consequently, resulted in overestimation in matric suction compared to their laboratory experimental observations. Figure 5a also illustrates that, early in the morning, due to the low atmospheric demand, matric suction is only increased for a few millimeters below the soil surface; however, later in the day, suction increases at deeper depths since the atmospheric demand is higher. This implies evaporation occurs from the deeper soil layers in the afternoon in comparison to the early morning. It is also observed that the maximum matric suction is always observed at the soil surface.

Figure 5b depicts the corresponding relative humidity of the soil which depends on matric suction through Kelvin's law ($RH = \exp[\psi M_w/(RT\rho_l)]$). It is understood that only high matric suction values decrease the relative humidity to values lower than unity. Therefore, the matric suctions calculated by NEPC approach do not affect the relative humidity of the soil except the afternoon of the last day in which it is decreased to $\approx$0.92. On the contrary, EPC approach predicts lower relative humidity on the first and last of the experiment, where the minimum calculated relative humidity is as low as 0.45 in the afternoon of the first day.

In Figure 5c, temperature changes are shown in the top 50 cm of the soil. Both models yield almost similar temperature variations except in the afternoon of the first day, where this discrepancy reaches to the depths of about $z = -30$ cm. As it can be seen in the figure EPC model predicts lower temperature. The reason can be because of the high matric suction at 16:00 of the first day predicted by EPC model which leads to development of a thin dry layer immediately below the surface while such dry layer is not developed in the first day according to NEPC approach calculations. As the thermal conductivity decreases for dry layers of soils (Figure 1); therefore, the ability to transfer heat from the atmospheric heat sink to deeper layers of the soil would be reduced which results in lower temperature variations.

In Figure 5d, the nonequilibrium and equilibrium vapor densities, which are calculated by NEPC and EPC models, respectively, are presented for different times of the first and last day. Equilibrium vapor density highly depends on the magnitude of matric suction and temperature of soils, while the nonequilibrium

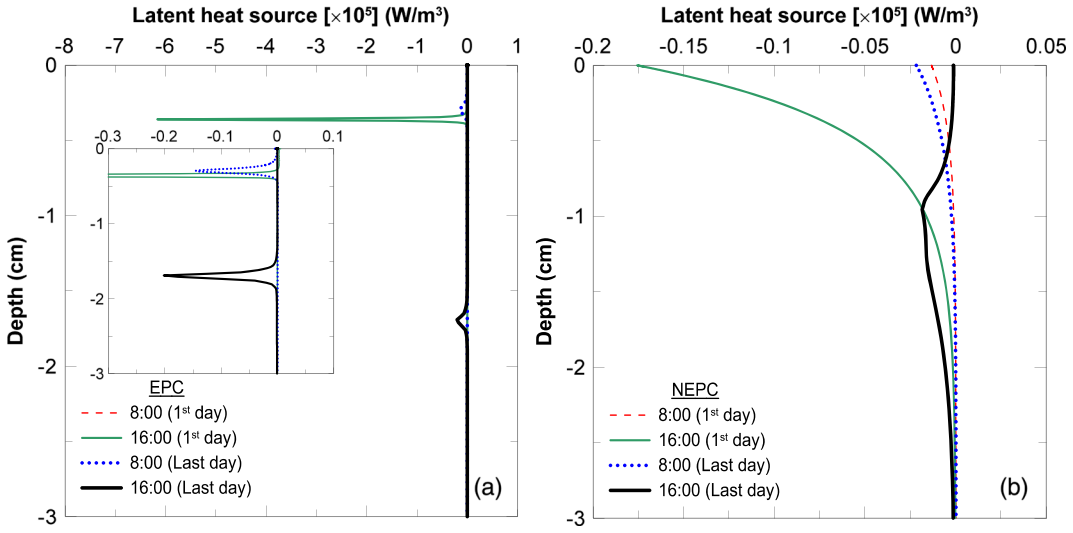

Figure 6. Latent heat source for selected times of the first and last day of the experiment: (a) EPC latent heat source and (b) NEPC latent heat source.

vapor density as an independent variable is not only affected by matric suction and temperature variations but also by the explicit expression of phase change rate defined in Equation 12. For the first day of the experiment, as shown in Figure 5d, the magnitude of nonequilibrium (actual) vapor density is lower than its equilibrium value for few millimeters of the top layer of the soil at 8:00. As both models yield relatively similar matric suction, relative humidity, and temperature changes for this particular time; therefore, the difference between the vapor densities may be associated with nonequilibrium and EPC rates. This will be elaborated later in more detail. In the morning of the last day, the equilibrium vapor density is slightly smaller than the one obtained by nonequilibrium model for depths above $z = -0.5$ cm due to the slightly lower temperature changes predicted by EPC model, while relative humidity for both models is 1.However, in the vicinity of the atmospheric boundary, the reverse behavior is observed. Later in the afternoon of the first day, calculated equilibrium vapor density is lower than the nonequilibrium one below $z = -0.5$ cm, because the lower temperature predicted by EPC results in smaller saturated vapor density (please see the definition of saturated vapor density in Table 1) and consequently the lower equilibrium vapor density. A distinct change of slope above $z = -0.5$ cm in the calculated equilibrium vapor density is evident from the fact that relative humidity from this point upward is strongly decreased. Same trend is observed in the afternoon of the last day for equilibrium vapor density except the change of slope occurs deeper at about $z = -1.75$ cm. Same shift is evident for nonequilibrium vapor densities in both days at 16:00, but there is no drastic change in the slope.

Figure 6 displays the latent heat source in the soil domain (i.e., right-hand side of the Equations 10 and 15, respectively, for NEPC and EPC approaches) to better illustrate how EPC and NEPC rates happen in shallow depths. The negative sign shows the evaporation, whereas the positive sign shows the condensation process. On the first day at 8:00 am, no evaporative process can be observed from EPC model; on the other hand, NEPC approach shows low evaporation at and close to the surface. Later for the same day at 16:00, an extremely high evaporation magnitude yet in a very narrow zone can be seen at about $z = -0.3$ cm in EPC model estimation. In comparison, for NEPC approach, a very wide zone of evaporation from the surface is evident which is extended to $z = -2$ cm but in much lower magnitude in comparison to EPC model. The reason for different evaporative behavior obtained from NEPC approach can be investigated by referring to Equation 13, in which the interfacial area is zero when soil is completely dry ($S_l = 0$) and it reaches to the maximum value when soil retains very small saturating liquid ($S_l = 1\%$). Furthermore, according to the HKS phase change model, the rate of phase change is proportional to the square root of the soil's temperature which further explains the dynamics of the phase change throughout the day with variations of temperature in soil as shown in Figure 5c.

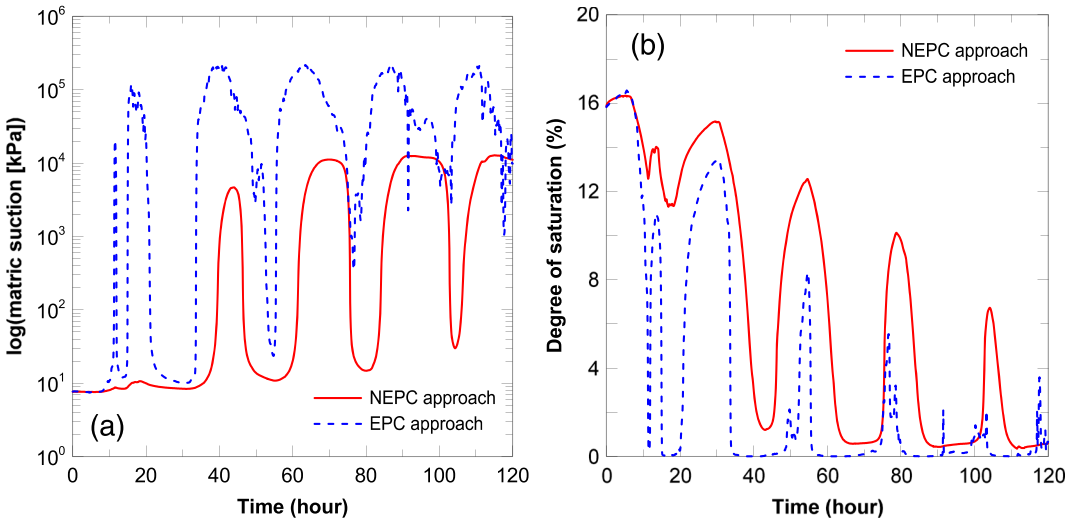

Figure 7. The simulated (a) matric suction and (b) liquid degree of saturation at the top the soil boundary versus the time of the experiment.

In the morning of the last day, same narrow evaporation zone close to the surface is simulated by EPC approach but much lower magnitude with respect to the evaporation at the same time in the first day. This behavior refers to the point that the top layer of the soil has been resaturated in the morning time (because evaporation takes place in close to the surface); however, the liquid water availability is not as much as the first day of the experiment; hence, the evaporation magnitude is lower. Similarly, NEPC model shows low magnitude on evaporation, but the influential zone is wider than in EPC model. Later in the afternoon, both models estimate that the evaporation zone recedes deeper in the ground where the plateau of the NEPC latent heat of evaporation is about eight times lower than the one estimated by EPC model.

The evaporation/condensation from soil's subsurface is the source of alterations in the matric suction. Figure 7a shows the variations of the calculated matric suction at the soil surface with time\ and with respect to both EPC and NEPC approaches (temperature-modified Lu SWR model is incorporated in Both approaches). The fluctuation occurs due to the daily variations of atmospheric evaporative demand. The high suction gradients due to drying/wetting phase cycles are smoothly predicted using both

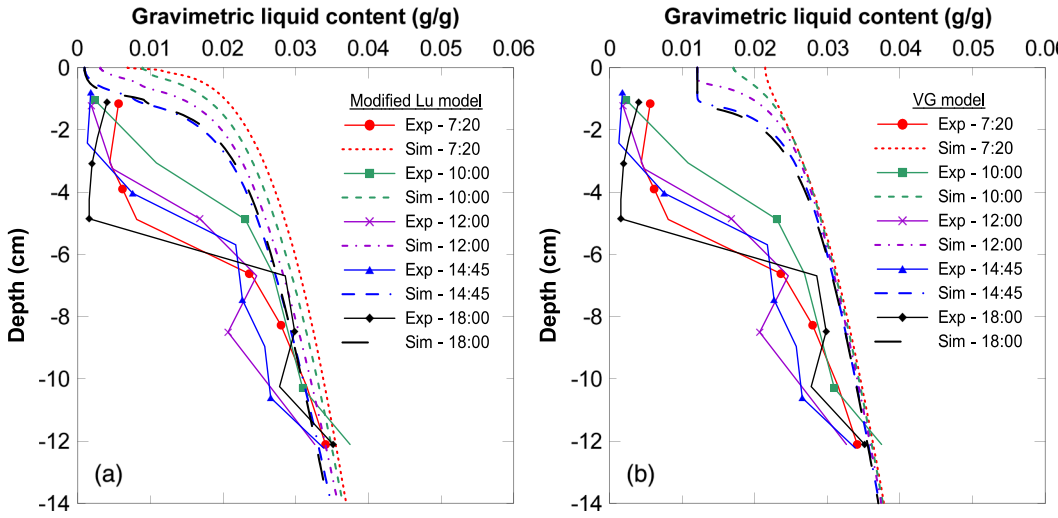

Figure 8. Variations of gravimetric liquid content in shallow depth of the soil on the last day of the experiment and the comparison of the simulations (NEPC) with the measured ones by Assouline et al. (2013): (a) temperature-modified Lu and (b) van Genuchten models.

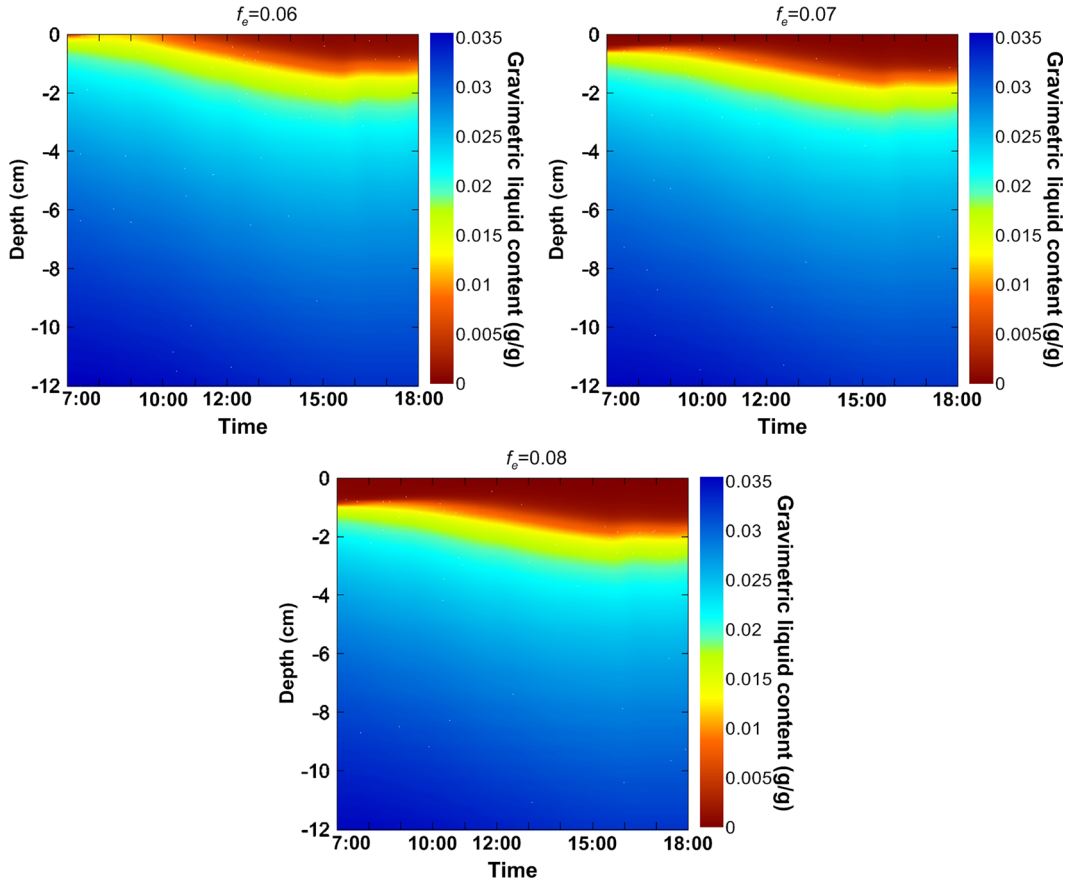

Figure 9. 1D schematic representation of the gravimetric liquid content in shallow depth of the soil on the last day with respect to different evaporation coefficients.

modeling approaches which implies the advantage of the hydraulic conductivity model with respect to capillary and film flow. This conclusion emphasizes the importance of the film flow in numerical modeling of nonisothermal multiphase flow to capture wetting/drying cycles below the residual liquid content with high matric suction. It is observed that the definition of film flow is necessary for numerical modeling convergence while dealing with high matric suction in dry-out zones. As explained earlier, EPC model impose a higher matric suction comparing to NEPC model, especially in the first heating phase. Figure 7b illustrates the changes in degree of saturation of liquid water at the soil surface with time. The gradual decrease in liquid degree of saturation after each wetting/drying cycle is evident from this figure. It is shown that EPC model leads to a faster and stronger desaturation with a weaker resaturation of the surface in comparison to NEPC model.

For the next step, NEPC model is used to analyze the dynamics of the gravimetric liquid content at the shallow subsurface during the bare soil evaporation. Figures 8a and 8b show the variation of gravimetric liquid content in the last day of the experiment in the vicinity of the soil-atmosphere boundary with the comparison between temperature-modified Lu and VG SWR models. According to Assouline et al. (2013), the gravimetric liquid content experimental data were measured in the laboratory from the destructive sampling that was performed at the end of the experiment. Please note in-filed and laboratory liquid water measurements are compared separately in Figures 3 and 8, respectively. In Figure 8a, numerical results show that the gravimetric liquid content at the vicinity of the soil-atmosphere boundary stays below the residual value with a small resaturation between 7:20 and 10:00 am at the top boundary. The evaporation results in reduction of liquid content and thickening of the dry soil layer below the subsurface. In contrast to the Lu SWR model's predictions, Figure 8b emphasize on the inability of the VG model to capture the moisture dynamics below the residual liquid content; however, VG model simulates the thickening of the dry soil layer below the subsurface.

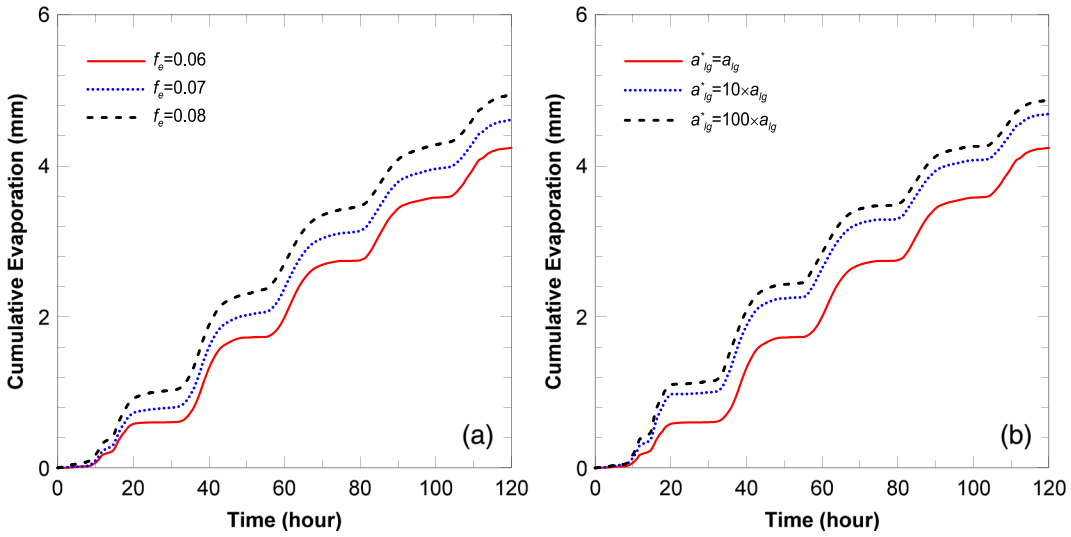

Figure 10. The effect of different (a) evaporation coefficient values and (b) liquid-gas interfacial area on the cumulative evaporation.

Although, NEPC model overestimates the gravimetric liquid content at the top layer compared to field measurements, but it shows the ability of the model to reasonably capture the dry state during the bare soil evaporation (in case of using a SWR model with the ability to capture the oven-dried saturation states). The reason for the overestimated gravimetric liquid content is further investigated through a sensitivity analysis which is done by considering different evaporation coefficients (f_e = 0.07 and 0.08). Figure 9 provides the gravimetric liquid content contours with depth at different times. It can be perceived from Figure 9 that increasing f_e will result in development of a thicker dry layer of soil. This comparison confirms the capability of the present model to capture the evaporation from deeper soil with proper incorporation of the SWR model. However, increasing f_e may lead to higher cumulative evaporation.

Figures 10a and 10b show the effects of larger evaporation coefficient (f_e) and liquid-gas interfacial area (a_{lg}) on the cumulative evaporation. The comparison of Figures 9 and 10a shows higher f_e results in better estimation of thicker dry soil layer at the last day of the experiment, while it overestimates the accumulative evaporation for the 5 days. This comparison indicates that evaporation coefficient may not be constant throughout the evaporation process as it may depend on liquid content and temperature of the soil. Same conclusion has been drawn by Trautz et al. (2015). However, proposing accurate evaporation coefficient needs much effort and is beyond the scope of this paper. Further investigation on the basis of NEPC approach is needed to understand the nonisothermal drying of the topsoil layers subjected to diurnal atmospheric conditions. Figure 10b demonstrates that larger liquid-gas interfacial areas result in higher cumulative evaporation. In general, by referring to Equation 12, increasing the liquid-gas interfacial area (or the mass transfer rate coefficient) to an infinitely large number forces the system to reach EPC condition. The latter was denoted by Li, Vanderborght, and Smits (2019). In present study, when $a_{lg}^* = 100 \times a_{lg}$, EPC is almost obtained.

5. Conclusion

In this study, the nonisothermal multiphase flow in shallow subsurface is carefully examined by utilizing NEPC approach. In the interest of comparison with NEPC approach, conventional EPC approach is also considered to point out the main differences of the two theoretical models. The developed models are incorporated in a finite element model to simulate the experimental observations of the evaporation from a fine sandy soil which was performed at the EPFL in 2006. During this experiment, soil was subjected to dynamic atmospheric conditions which enabled us to analyze the capability of NEPC approach with respect to the in-field evaporation process. Considering NEPC approach relaxes the restriction of the vapor density to be always equal to its equilibrium value. NEPC approach yields different matric suction, relative humidity, temperature, and evaporation/condensation behavior in a few centimeters below the soil surface than

EPC approach. Moreover, NEPC approach curbs the intense and highly localized phase change zone predicted by EPC through the macroscopic HKS phase change model. This marks the main difference of the two modeling approaches. The proposed (NEPC) model shows that evaporation from bare soil can be predicted with reasonable accuracy without using the enhancement factor nor knowing the depth of the vaporization plane. It is also found that, to capture the dynamics of fluid flow and liquid content due to the dry-out evaporation process, hydraulic conductivity of the film flow and the generalized SWR model to account for capillary and adsorption regime (temperature-modified Lu model is considered here) are significant. The evaporation/condensation coefficients are key parameters in controlling the evaporation rate. Although the constant values for evaporation/condensation coefficients considered in this study lead to rational results, further research is needed to analysis their dependency on state variables, such as temperature and volumetric liquid content.

Appendix A.

Surface albedo and soils surface emissivity depend on the surface volumetric liquid content, $\theta_{l,top}$, and are formulated as below.

$$\begin{cases} \alpha_{alb} = 0.25 & \theta_{l,\,top} < 0.1 \\ \alpha_{alb} = 0.1 & \theta_{l,\,top} < 0.25 \\ \alpha_{alb} = 0.35 - \theta_{l,\,top} & 0.1 \le \theta_{l,\,top} < 0.25 \end{cases} \tag{A1}$$

$$\varepsilon_s = \min\left(0.90 + 0.18\theta_{l,\,top}; 1.0\right) \tag{A2}$$

Atmospheric emissivity is defined as follows:

$$\varepsilon_a = 0.70 + 5.95 \times 10^{-5} e_a \exp\left(\frac{1500}{T_a}\right), \tag{A3}$$

$$e_a = 0.611\exp\left[\frac{17.27(T_a - 273.15)}{T_a - 35.85}\right] RH_a, \tag{A4}$$

where T_a is expressed in Kelvin. e_a (kPa) is the atmospheric vapor pressure, and RH_a is the relative humidity of the air which is given in Appendix B. The cloud factor is calculated from the atmospheric transmission coefficient for solar radiation, T_t:

$$0 \le c_f = 2.33 - 3.33T_t \le 1, \tag{A5}$$

$$T_t = \frac{S_n}{Q_p}. \tag{A6}$$

$Q_p = 1{,}360 \times \cos\theta$ (W/m^2) is the potential daily global solar radiation, and θ is solar elevation zenith angle given by

$$\cos\theta = \sin\lambda\sin\delta + \cos\lambda\cos\delta[0.2618(t - t_0)], \tag{A7}$$

$$\sin\delta = 0.3985\sin\left[2\pi\frac{\mathrm{DOY}}{365} - 1.414 + 0.03345\sin\left(6.224 + \pi\frac{\mathrm{DOY}}{365}\right)\right]. \tag{A8}$$

In Equation A7, λ is the latitude, δ is the solar declination, t is time, and t_0 is the time of solar noon. In Equation A8, DOY represents a day of the year.

Appendix B.

The micrometeorological data which are used to model the lysimeter test are presented in Figure B1

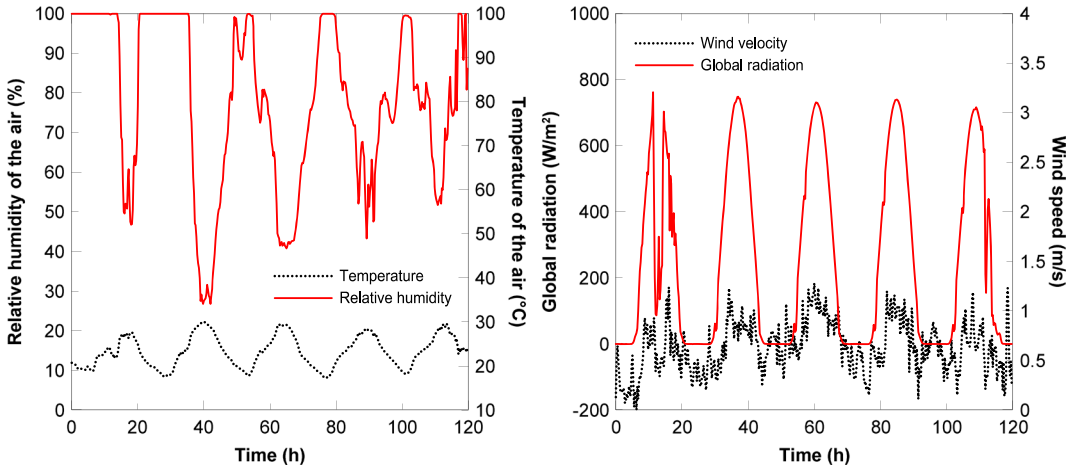

Figure B1. The climate data used to simulate the atmospheric condition: relative humidity and temperature of the air (left), global radiation and wind velocity (right).

Nomenclature

M (−)	Adsorption strength
θ_a (m^3/m^3)	Adsorption volumetric content
r_H (s/m)	Aerodynamic resistance to heat transfer
r_v (s/m)	Aerodynamic resistant to mass transfer
C_v ($J/m^3/K$)	Air volumetric heat capacity
α (1/Pa)	Air-entry parameter
ε_a (−)	Atmospheric emissivity
p_a (Pa)	Atmospheric pressure
δ (−)	Atmospheric stability factor
D_v^0 (m^2/s)	Binary diffusion coefficient of vapor in gas phase
k_b (J/K)	Boltzmann constant
k_{cap} (m/s)	Capillary hydraulic conductivity
θ_c (m^3/m^3)	Capillary volumetric content
c_f (−)	Cloud factor
f_c (−)	Condensation coefficient
d (m)	Constant parameter
f (−)	Correction factor
μ_g (Pa·s)	Dynamic viscosity of gas
μ_l (Pa·s)	Dynamic viscosity of liquid
ρ_m (kg/m^3)	Effective density of medium
D_v (m^2/s)	Effective diffusivity
d_g (m)	Effective grain diameter
C_m (J/kg/K)	Effective heat capacity of medium
λ_m ($W/m^2/K$)	Effective thermal conductivity of medium
a (C)	Electron charge
$\rho_{v,eq}$ (kg/m^3)	Equilibrium vapor density
$(\rho_{v,eq})_a$ (kg/m^3)	Equilibrium vapor density of air
f_e (−)	Evaporation coefficient
k_{film} (m/s)	Film flow hydraulic conductivity
c (−)	Fitting parameter

α_{1-4} (−)	Fitting parameters
q_g (kg/m^2/s)	Gas advective flux
ρ_g (kg/m^3)	Gas density
p_g (Pa)	Gas pressure
S_g (−)	Gas saturation degree
$\psi_{\max}$ (Pa)	Highest suction
S_n (W/m^2)	Incoming solar radiation
κ_{int} (m^2)	Intrinsic permeability
L_v (J/kg)	Latent heat of vaporization
q_l (kg/m^2/s)	Liquid advective flux
ρ_l (kg/m^3)	Liquid density
S_l (−)	Liquid saturation degree
z_i (−)	Magnitude of the ionic charge
κ_{lg} (m/s)	Mass transfer rate coefficient
ψ (Pa)	Matric suction
$\theta_{\text{a,max}}$ (m^3/m^3)	Maximum adsorption capacity
ψ_{cav} (Pa)	Mean cavitation suction
M_a (kg/mol)	Molecular weight of dry air
M_w (kg/mol)	Molecular weight of liquid
R_{nl} (W/m^2)	Net longwave radiation
R_{ns} (W/m^2)	Net shortwave radiation
ε_0 (C^2/J/m)	Permittivity of free space
$\dot{m}$ (kg/m^3/s)	Phase change rate
p_l (Pa)	Pore liquid pressure
n (m^3/m^3)	Porosity
z_{ref} (m)	Reference height
T_{ref} (K)	Reference temperature
RH (−)	Relative humidity
κ_{rg} (−)	Relative permeability of gas
κ_{rl} (−)	Relative permeability of liquid
ε (−)	Relative permittivity of water
k_{s} (m/s)	Saturated hydraulic conductivity
$\rho_{v,sat}$ (kg/m^3)	Saturated vapor density
H (W/m^2)	Sensible heat flux
ε_{s} (−)	Soil surface emissivity
R_{n} (W/m^2)	Solar radiation
a_{lg} (1/m)	Liquid-gas interfacial area
σ_{cav} (Pa)	Standard deviation for cavitation
σ_s (W/m^2/K^4)	Stefan-Boltzmann's law of radiation constant
α_{alb} (−)	Surface albedo
G (W/m^2)	Surface heat flux
z_0 (m)	Surface roughness
σ (Pa/m)	Surface tension
T (K)	Temperature
τ (−)	Tortuosity
R (Pa·m^3/K/mol)	Universal gas constant
ρ_v (kg/m^3)	Vapor density
E (kg/m^2/s)	Vapor flux
n_{VG} (−)	VG parameter
m_{VG} (−)	VG parameter
θ_g (m^3/m^3)	Volumetric gas content
θ_l (m^3/m^3)	Volumetric liquid content
κ (−)	von Karman constant
υ (m/s)	Wind speed

Data Availability Statement

All the meteorological, and experimental data are available through Assouline et al. (2013) and Mehta et al. (1994). The Experimental datasets used in this study are included in the paper in Figures 2a, 3, 4, and 8 and in Appendices A and B. The results of numerical model used during the study appear in the submitted article.

Acknowledgments
The authors would like to gratefully acknowledge the financial support by the National Science Foundation under Grant CMMI-1804822. Authors would also like to thank Dr Shmuel Assouline who provided the micrometeorological data measured in the field.

References

Araújo, J. B., & Brusseau, M. L. (2019). Novel fluid–fluid interface domains in geologic media. *Environmental Science: Processes & Impacts*, *21*(1), 145–154.

Assouline, S., Narkis, K., Gherabli, R., Lefort, P., & Prat, M. (2014). Analysis of the impact of surface layer properties on evaporation from porous systems using column experiments and modified definition of characteristic length. *Water Resources Research*, *50*, 3933–3955. https://doi.org/10.1002/2013WR014489

Assouline, S., Tyler, S. W., Selker, J. S., Lunati, I., Higgins, C., & Parlange, M. (2013). Evaporation from a shallow water table: Diurnal dynamics of water and heat at the surface of drying sand. *Water Resources Research*, *49*, 4022–4034. https://doi.org/10.1002/wrcr.20293

Bear, J. (2013). *Dynamics of Fluids in Porous Media*. Mineola, NY: Courier Corporation.

Benet, J.-C., Lozano, A.-L., Cherblanc, F., & Cousin, B. (2009). Phase change of water in a hygroscopic porous medium. Phenomenological relation and experimental analysis for water in soil. *Journal of Non-Equilibrium Thermodynamics*, *34*(2), 133–153.

Bittelli, M., Campbell, G. S., & Tomei, F. (2015) *Soil Physics with Python: Transport in the Soil-Plant-Atmosphere System*. New York, NY: Oxford University Press. https://doi.org/10.1093/acprof:oso/9780199683093.001.0001

Bittelli, M., Ventura, F., Campbell, G. S., Snyder, R. L., Gallegati, F., & Pisa, P. R. (2008). Coupling of heat, water vapor, and liquid water fluxes to compute evaporation in bare soils. *Journal of Hydrology*, *362*(3–4), 191–205. https://doi.org/10.1016/j.jhydrol.2008.08.014

Brutsaert, W. (2005). *Hydrology: An Introduction*. New York, NY: Cambridge University Press. https://doi.org/10.1017/CBO9780511808470

Brutsaert, W. (2015). A generalized complementary principle with physical constraints for land-surface evaporation. *Water Resources Research*, *51*, 8087–8093. https://doi.org/10.1002/2015WR017720

Campbell, G., Jungbauer, J. Jr., Bidlake, W., & Hungerford, R. (1994). Predicting the effect of temperature on soil thermal conductivity. *Soil Science*, *158*(5), 307–313. https://doi.org/10.1097/00010694-199411000-00001

Cass, A., Campbell, G., & Jones, T. (1984). Enhancement of thermal water vapor diffusion in soil 1. *Soil Science Society of America Journal*, *48*(1), 25–32. https://doi.org/10.2136/sssaj1984.03615995004800010005x

Chammari, A., Naon, B., Cherblanc, F., & Benet, J. (2003). Water transport with phase change at low water content. *Comptes Rendus Mecanique*, *331*(11), 759–765. https://doi.org/10.1016/j.crme.2003.07.005

Chapuis, R. P., & Aubertin, M. (2003). On the use of the Kozeny Carman equation to predict the hydraulic conductivity of soils. *Canadian Geotechnical Journal*, *40*(3), 616–628. https://doi.org/10.1139/t03-013

Choudhury, B., Reginato, R., & Idso, S. (1986). An analysis of infrared temperature observations over wheat and calculation of latent heat flux. *Agricultural and Forest Meteorology*, *37*(1), 75–88. https://doi.org/10.1016/0168-1923(86)90029-8

Class, H., Helmig, R., & Bastian, P. (2002). Numerical simulation of non-isothermal multiphase multicomponent processes in porous media: 1. An efficient solution technique. *Advances in Water Resources*, *25*(5), 533–550. https://doi.org/10.1016/S0309-1708(02)00014-3

Costanza-Robinson, M. S., & Brusseau, M. L. (2002). Air-water interfacial areas in unsaturated soils: Evaluation of interfacial domains. *Water Resources Research*, *38*(10), 1195. https://doi.org/10.1029/2001WR000738

Dijkema, J., Koonce, J., Shillito, R., Ghezzehei, T., Berli, M., Van Der Ploeg, M., & Van Genuchten, M. T. (2018). Water distribution in an arid zone soil: Numerical analysis of data from a large weighing lysimeter. *Vadose Zone Journal*, *17*(1), 170035. https://doi.org/10.2136/vzj2017.01.0035

Fetzer, T., Smits, K. M., & Helmig, R. (2016). Effect of turbulence and roughness on coupled porous-medium/free-flow exchange processes. *Transport in Porous Media*, *114*(2), 395–424. https://doi.org/10.1007/s11242-016-0654-6

Fetzer, T., Vanderborght, J., Mosthaf, K., Smits, K. M., & Helmig, R. (2017). Heat and water transport in soils and across the soil-atmosphere interface: 2. Numerical analysis. *Water Resources Research*, *53*, 1080–1100. https://doi.org/10.1002/2016WR019983

Gao, B., Davarzani, H., Helmig, R., & Smits, K. M. (2018). Experimental and Numerical Study of Evaporation From Wavy Surfaces by Coupling Free Flow and Porous Media Flow. *Water Resources Research*, *54*, 9096–9117. https://doi.org/10.1029/2018WR023423

Grant, S. A., & Salehzadeh, A. (1996). Calculation of temperature effects on wetting coefficients of porous solids and their capillary pressure functions. *Water Resources Research*, *32*(2), 261–270. https://doi.org/10.1029/95WR02915

Haghighi, E., & Kirchner, J. W. (2017). Near-surface turbulence as a missing link in modeling evapotranspiration-soil moisture relationships. *Water Resources Research*, *53*(7), 5320–5344. https://doi.org/10.1002/2016WR020111

Herbert, E., Balibar, S., & Caupin, F. (2006). Cavitation pressure in water. *Physical Review E*, *74*(4), 041603. https://doi.org/10.1103/PhysRevE.74.041603

Hillel, D. (2013). *Introduction to Soil Physics*, New York, NY: Academic press.

Hruška, M., Clauser, C., & De Doncker, R. W. (2019). Influence of dry ambient conditions on performance of underground medium-voltage DC cables. *Applied Thermal Engineering*, *149*, 1419–1426. https://doi.org/10.1016/j.applthermaleng.2018.11.076

Jafari, P., Masoudi, A., Irajizad, P., Nazari, M., Kashyap, V., Eslami, B., & Ghasemi, H. (2018). Evaporation mass flux: A predictive model and experiments. *Langmuir*, *34*(39), 11676–11684. https://doi.org/10.1021/acs.langmuir.8b02289

Jiang, H., Guo, B., & Brusseau, M. L. (2020). Pore-scale Modeling of fluid-fluid interfacial area in variably saturated porous media containing microscale surface roughness. *Water Resources Research*, *56*(1). https://doi.org/10.1029/2019WR025876

Joekar-Niasar, V., Hassanizadeh, S., & Leijnse, A. (2008). Insights into the relationships among capillary pressure, saturation, interfacial area and relative permeability using pore-network modeling. *Transport in Porous Media*, *74*(2), 201–219. https://doi.org/10.1007/s11242-007-9191-7

Kroener, E., Vallati, A., & Bittelli, M. (2014). Numerical simulation of coupled heat, liquid water and water vapor in soils for heat dissipation of underground electrical power cables. *Applied Thermal Engineering*, *70*(1), 510–523. https://doi.org/10.1016/j.applthermaleng.2014.05.033

Kryukov, A., & Levashov, V. Y. (2011). About evaporation–condensation coefficients on the vapor–liquid interface of high thermal conductivity matters. *International Journal of Heat and Mass Transfer*, *54*(13–14), 3042–3048. https://doi.org/10.1016/j.ijheatmasstransfer.2011.02.042

Li, Y., Kustas, W. P., Huang, C., Nieto, H., Haghighi, E., Anderson, M. C., et al. (2019). Evaluating soil resistance formulations in thermal-based two-source energy balance (TSEB) model: Implications for heterogeneous semiarid and arid regions. *Water Resources Research*, *55*, 1059–1078. https://doi.org/10.1029/2018WR022981

Li, Z., Vanderborght, J., & Smits, K. M. (2019). Evaluation of model concepts to describe water transport in shallow subsurface soil and across the soil–air interface. *Transport in Porous Media*, *128*(3), 945–976. https://doi.org/10.1007/s11242-018-1144-9

Lu, N. (2016). Generalized soil water retention equation for adsorption and capillarity. *Journal of Geotechnical and Geoenvironmental Engineering*, *142*(10), 04016051. https://doi.org/10.1061/(ASCE)GT.1943-5606.0001524

Lu, N., & Likos, W. J. (2004). *Unsaturated Soil Mechanics*. Hoboken, New Jersey: Wiley.

Marek, R., & Straub, J. (2001). Analysis of the evaporation coefficient and the condensation coefficient of water. *International Journal of Heat and Mass Transfer*, *44*(1), 39–53. https://doi.org/10.1016/S0017-9310(00)00086-7

Massman, W. (2015). A non-equilibrium model for soil heating and moisture transport during extreme surface heating: The soil (heat-moisture-vapor) HMV-model version. *Geoscientific model Development*, *8*. 3659–3680. 8, 3659–3680

Mehta, B. K., Shiozawa, S., & Nakano, M. (1994). Hydraulic properties of a sandy soil at low water contents. *Soil Science*, *157*(4), 208–214. https://doi.org/10.1097/00010694-199404000-00002

Millington, R., & Quirk, J. (1961). Permeability of porous solids. *Transactions of the Faraday Society*, *57*, 1200–1207. https://doi.org/10.1039/tf9615701200

Milly, P. C. D. (1982). Moisture and heat transport in hysteretic, inhomogeneous porous media: A matric head-based formulation and a numerical model. *Water Resources Research*, *18*(3), 489–498. https://doi.org/10.1029/WR018i003p00489

Mohanty, B., Shouse, P., & van Genuchten, M. T. (1998). Spatio-temporal dynamics of water and heat in a field soil. *Soil and Tillage Research*, *47*(1–2), 133–143. https://doi.org/10.1016/S0167-1987(98)00084-1

Monteith, J., & Unsworth, M. (2013). *Principles of Environmental Physics: Plants, Animals, and the Atmosphere*. Burlington, MA: Academic Press.

Moradi, A., Smits, K. M., Lu, N., & McCartney, J. S. (2016). Heat transfer in unsaturated soil with application to borehole thermal energy storage. *Vadose Zone Journal*, *15*(10), vzj2016.03.0027. https://doi.org/10.2136/vzj2016.03.0027

Mosthaf, K., Baber, K., Flemisch, B., Helmig, R., Leijnse, A., Rybak, I., & Wohlmuth, B. (2011). A coupling concept for two-phase compositional porous-medium and single-phase compositional free flow. *Water Resources Research*, *47*, W10522. https://doi.org/10.1029/2011WR010685

Mosthaf, K., Helmig, R., & Or, D. (2014). Modeling and analysis of evaporation processes from porous media on the REV scale. *Water Resources Research*, *50*, 1059–1079. https://doi.org/10.1002/2013WR014442

Nguyen, T. S., Li, Z., Barnichon, J., & Garitte, B. J. E. G. (2017). Modelling a heater experiment for radioactive waste disposal. *Environmental Geotechnics*, *4*(2).

Niessner, J., & Hassanizadeh, S. M. (2009a). Modeling kinetic interphase mass transfer for two-phase flow in porous media including fluid–fluid interfacial area. *Transport in Porous Media*, *80*(2), 329–344. https://doi.org/10.1007/s11242-009-9358-5

Niessner, J., & Hassanizadeh, S. M. (2009b). Non-equilibrium interphase heat and mass transfer during two-phase flow in porous media—Theoretical considerations and modeling. *Advances in Water Resources*, *32*(12), 1756–1766. https://doi.org/10.1016/j.advwatres.2009.09.007

Novak, M. D. (2010). Dynamics of the near-surface evaporation zone and corresponding effects on the surface energy balance of a drying bare soil. *Agricultural and Forest Meteorology*, *150*(10), 1358–1365. https://doi.org/10.1016/j.agrformet.2010.06.005

Novak, M. D. (2016). Importance of soil heating, liquid water loss, and vapor flow enhancement for evaporation. *Water Resources Research*, *52*, 8023–8038. https://doi.org/10.1002/2016WR018874

Novak, M. D. (2019). Validity of assuming equilibrium between liquid water and vapor for simulating evaporation. *Water Resources Research*, *55*, 9858–9872. https://doi.org/10.1029/2019WR025113

Nuske, P., Joekar-Niasar, V., & Helmig, R. (2014). Non-equilibrium in multiphase multicomponent flow in porous media: An evaporation example. *International Journal of Heat and Mass Transfer*, *74*, 128–142. https://doi.org/10.1016/j.ijheatmasstransfer.2014.03.011

Or, D., Lehmann, P., Shahraeeni, E., & Shokri, N. J. V. Z. J. (2013). Advances in soil evaporation physics—A review. *Vadose Zone Journal*, *12*(4).

Or, D., & Tuller, M. (1999). Liquid retention and interfacial area in variably saturated porous media: Upscaling from single-pore to sample-scale model. *Water Resources Research*, *35*(12), 3591–3605. https://doi.org/10.1029/1999WR900262

Ouedraogo, F., Cherblanc, F., Naon, B., & Bénet, J.-C. (2013). Water transfer in soil at low water content. Is the local equilibrium assumption still appropriate? *Journal of Hydrology*, *492*, 117–127. https://doi.org/10.1016/j.jhydrol.2013.04.004

Peng, S., & Brusseau, M. L. (2005). Impact of soil texture on air-water interfacial areas in unsaturated sandy porous media. *Water Resources Research*, *41*. https://doi.org/10.1029/2004WR003233

Persad, A. H., & Ward, C. A. (2016). Expressions for the evaporation and condensation coefficients in the Hertz-Knudsen relation. *Chemical Reviews*, *116*(14), 7727–7767. https://doi.org/10.1021/acs.chemrev.5b00511

Philip, J., & De Vries, D. (1957). Moisture movement in porous materials under temperature gradients. *Eos, Transactions American Geophysical Union*, *38*(2), 222–232. https://doi.org/10.1029/TR038i002p00222

Revil, A., & Lu, N. (2013). Unified water isotherms for clayey porous materials. *Water Resources Research*, *49*, 5685–5699. https://doi.org/10.1002/wrcr.20426

Saito, H., Šimůnek, J., & Mohanty, B. P. (2006). Numerical analysis of coupled water, vapor, and heat transport in the vadose zone. *Vadose Zone Journal*, *5*(2), 784–800. https://doi.org/10.2136/vzj2006.0007

She, H. Y., & Sleep, B. E. (1998). The effect of temperature on capillary pressure-saturation relationships for air-water and perchloroethylene-water systems. *Water Resources Research*, *34*(10), 2587–2597. https://doi.org/10.1029/98WR01199

Shokri, N., Lehmann, P., & Or, D. (2009). Critical evaluation of enhancement factors for vapor transport through unsaturated porous media. *Water Resources Research*, *45*, W10433. https://doi.org/10.1029/2009WR007769

Smits, K., Cihan, A., Sakaki, T., Howington, S., Peters, J., & Illangasekare, T. (2012). Experimental and modeling investigation of soil moisture and thermal behavior in the vicinity of buried objects. *IEEE Transactions on Geoscience and Remote Sensing*, *51*(5).

Smits, K. M., Cihan, A., Sakaki, T., & Illangasekare, T. H. (2011). Evaporation from soils under thermal boundary conditions: Experimental and modeling investigation to compare equilibrium-and nonequilibrium-based approaches. *Water Resources Research*, *47*, W05540. https://doi.org/10.1029/2010WR009533

Strati, V., Albéri, M., Anconelli, S., Baldoncini, M., Bittelli, M., Bottardi, C., et al. (2018). Modelling soil water content in a tomato field: Proximal gamma ray spectroscopy and soil–crop system models. *Agriculture*, *8*(4), 60. https://doi.org/10.3390/agriculture8040060

Sviercoski, R., Efendiev, Y., & Mohanty, B. J. W. R. R. (2018). Upscaling the coupled water and heat transport in the shallow subsurface. *Water Resources Research*, *54*, 995–1012. https://doi.org/10.1002/2017WR021490

Tamizdoust, M. M., & Ghasemi-Fare, O. (2020). A fully coupled thermo-poro-mechanical finite element analysis to predict the thermal pressurization and thermally induced pore fluid flow in soil media. *Computers and Geotechnics*, *117*, 103250. https://doi.org/10.1016/j.compgeo.2019.103250

Tokunaga, T. K. (2009). Hydraulic properties of adsorbed water films in unsaturated porous media. *Water Resources Research*, *45*, W06415. https://doi.org/10.1029/2009WR007734

Trautz, A. C., Smits, K. M., & Cihan, A. (2015). Continuum-scale investigation of evaporation from bare soil under different boundary and initial conditions: An evaluation of nonequilibrium phase change. *Water Resources Research*, *51*, 7630–7648. https://doi.org/10.1002/2014WR016504

van de Griend, A. A., & Owe, M. (1994). Bare soil surface resistance to evaporation by vapor diffusion under semiarid conditions. *Water Resources Research*, *30*(2), 181–188. https://doi.org/10.1029/93WR02747

Van Genuchten, M. T. (1980). A closed-form equation for predicting the hydraulic conductivity of unsaturated soils 1. *Soil Science Society of America Journal*, *44*(5), 892–898. https://doi.org/10.2136/sssaj1980.03615995004400050002x

Vanderborght, J., Fetzer, T., Mosthaf, K., Smits, K. M., & Helmig, R. (2017). Heat and water transport in soils and across the soil-atmosphere interface: 1. Theory and different model concepts. *Water Resources Research*, *53*, 1057–1079. https://doi.org/10.1002/2016WR019982

Vlasov, V. A. (2019). Modeling of evaporation and condensation processes: A chemical kinetics approach. *Heat and Mass Transfer*, *55*(6), 1661–1669. https://doi.org/10.1007/s00231-018-02549-y

Wagner, W. & Kretzschmar, H.-J. (2008). IAPWS industrial formulation 1997 for the thermodynamic properties of water and steam. International steam tables: Properties of water and steam based on the industrial formulation IAPWS-IF97, 7-150.

Whitaker, S. (1977). Simultaneous Heat, Mass, and Momentum Transfer in Porous Media: A Theory of Drying. *Advances in Heat Transfer*, *13*, 119–203.

Zhang, Z. F. (2011). Soil water retention and relative permeability for conditions from oven-dry to full saturation. *Vadose Zone Journal*, *10*(4), 1299–1308. https://doi.org/10.2136/vzj2011.0019